

Spatiotemporal relationships between sea level pressure and air temperature in the tropics

A. M. Makarieva^{1,2*}, V. G. Gorshkov^{1,2}, A.V. Nefiodov¹,
D. Sheil^{3,4,5,6}, A. D. Nobre⁷, B.-L. Li²

¹Theoretical Physics Division, Petersburg Nuclear Physics Institute, 188300 Gatchina, St. Petersburg, Russia ²XIEG-UCR International Center for Arid Land Ecology, University of California, Riverside 92521-0124, USA ³Norwegian University of Life Sciences, Ås, Norway ⁴School of Environment, Science and Engineering, Southern Cross University, PO Box 157, Lismore, NSW 2480, Australia; ⁵Institute of Tropical Forest Conservation, Mbarara University of Science and Technology, PO Box, 44, Kabale, Uganda; ⁶Center for International Forestry Research, PO Box 0113 BOCBD, Bogor 16000, Indonesia; ⁷Centro de Ciência do Sistema Terrestre INPE, São José dos Campos SP 12227-010, Brazil.

Abstract

While surface temperature gradients have been highlighted as drivers of low-level atmospheric circulation, the underlying physical mechanisms remain unclear. Lindzen and Nigam (1987) noted that sea level pressure (SLP) gradients are proportional to surface temperature gradients if isobaric height (the height where pressure does not vary in the horizontal plane) is constant; their own model of low-level circulation assumed that isobaric height in the tropics is around 3 km. Recently Bayr and Dommenges (2013) proposed a simple model of temperature-driven air redistribution from which they derived that the isobaric height in the tropics again varies little but occurs higher (at the height of the troposphere). Here investigations show that neither the empirical assumption of Lindzen and Nigam (1987) nor the theoretical derivations of Bayr and Dommenges (2013) are plausible. Observations show that isobaric height is too variable to determine a universal spatial or temporal relationship between local values of air temperature and SLP. Since isobaric height cannot be determined from independent considerations, the relationship between SLP and temperature is not evidence that differential heating drives low-level circulation. An alternative theory suggests SLP gradients are determined by the condensation of water vapor as moist air converges towards the equator. This theory quantifies the meridional SLP differences observed by season across the Hadley cells reasonably well. Higher temperature of surface air where SLP is low may be determined by equatorward transport and release of latent heat below the trade wind inversion layer. The relationship between atmospheric circulation and moisture dynamics merits further investigation.

1 Introduction

Low-level tropical winds are generally linked to convection, but the physical processes and relationships remain a matter of interest and discussion. One question is whether the release of latent heat in the upper atmosphere generates sufficient moisture convergence in the lower atmosphere to feed convection. The observed relationship between sea surface temperature and SLP (with warm areas having low pressure) is regarded as evidence that low-level convergence is, rather, driven by the temperature gradients (see discussions by Lindzen and Nigam, 1987; Neelin, 1989; Sobel and Neelin, 2006; Back and Bretherton, 2009; An, 2011).

*Corresponding author. E-mail: ammakarieva@gmail.com

The central concept behind surface pressure gradients driven by surface differential heating in a hydrostatic atmosphere is the existence of an isobaric height — a certain pressure level with its altitude remaining constant in either space or time despite changing surface temperature and pressure. If such a level exists, in areas where temperature is high and air density is low there will be less air below the isobaric height than where temperature is low and air density is high. Accordingly, surface pressure equal to the weight of the air column will be lower in the warmer than in the colder areas. Moreover, the surface pressure and temperature gradients will be proportional to each other, with the proportionality coefficient set by the isobaric height.

The main problem is to find the isobaric height. While for a liquid a natural candidate is the height of the upper surface, our gaseous atmosphere lacks a sharp upper boundary. Lindzen and Nigam (1987) suggested that isobaric height in the tropics approximately coincides with the height of the trade wind inversion (≈ 3 km). However, no theoretical justifications were offered. More recently Bayr and Dommenges (2013) suggested the height of the troposphere could be isobaric. Specifically, Bayr and Dommenges (2013) proposed a simple physical model where air is re-distributed between air columns subjected to differential heating so as the height of a certain pressure level remains the same. From this model Bayr and Dommenges (2013) concluded that this constant height is the height of the troposphere at $H \approx 16$ km and that it determines the proportionality between changes of the mean tropospheric temperature and SLP.

So is the tropical isobaric height 3 km following Lindzen and Nigam (1987) or 16 km following Bayr and Dommenges (2013)? If we knew that a constant isobaric height exists in the tropics and could link its magnitude to known atmospheric parameters, we could use surface temperatures to predict surface pressures and, resulting from air circulation, moisture convergence and precipitation. Our incomplete understanding of the physical principles governing low-level circulation is manifested by the inability of atmospheric models to replicate the terrestrial water cycle (Marengo, 2006; Hagemann et al., 2011) as well as by the challenge of confidently predicting precipitation and air circulation under a changing climate (e.g., An, 2011; Huang et al., 2013).

To explore the relationship between surface pressure and temperature we start by re-examining the derivation of Bayr and Dommenges (2013). We identify and resolve several inconsistencies in their model (Section 2). We demonstrate that the height of the tropical troposphere is not an isobaric height and that it does not determine the ratio between the mean tropospheric temperature and SLP changes. We then derive a general relationship linking the ratio of gradients (as well as of temporal changes) of surface pressure and temperature to an isobaric height. We show that this ratio is a function not of one but of two heights, isobaric and isothermal (Section 3).

Using data provided by the National Centers for Environmental Prediction/National Center for Atmospheric Research (NCEP/NCAR) Reanalysis (Kalnay et al., 1996) and the Remote Sensing Systems (Mears and Wentz, 2009) we investigate the spatial and temporal relationships between tropical SLP and air temperature on a seasonal timescale (Section 4). These data show no constant isobaric height in the tropical atmosphere. The isobaric height (defined as the height where the meridional pressure gradient is zero) in fact grows sharply from zero around the 30th latitudes to above the tropospheric height at the equator. We show that the isobaric height varies with location and season.

We then demonstrate that in theory a constant isobaric height dictates a proportionality between pressure gradients at the surface and in the upper atmosphere irrespective of whether the latter are driven by differential heating at the surface or in the upper atmosphere. We demonstrate that in the real atmosphere such a proportionality does not exist (Section 5). We argue that the mere existence of a relationship between surface gradients of pressure and temperature does not by itself imply causality and is thus insufficient to conclude that surface pressure gradients are driven by differential heating.

We here propose an alternative concept to understand and quantify the observed sur-

face pressure variation in the tropics. Horizontal transport of moisture with its subsequent condensation and precipitation away from the point where it evaporated produces pressure gradients due to the changing air concentration as it moves from the evaporation to condensation area (Makarieva et al., 2013b, 2014a). Pressure is greater where water vapor is added and lower where it is removed from the air column. Horizontal moisture transport thus appears to be the direct cause of the surface pressure gradients that, in their turn, maintain this transport and the associated convection. This theoretical approach effectively describes the seasonal dynamics of surface pressure differences across the Hadley cells (Section 6). Finally, we show that the horizontal transport of moisture can also account for the association between the surface pressure and temperature gradients (Section 7).

2 The physical model of Bayr and Dommenges (2013)

Bayr and Dommenges (2013) begin their derivation with an equation they refer to as "the hydrostatic equation"

$$dp = -\rho g d\eta \quad (1)$$

with pressure p , density ρ , gravity constant g , and η described as "air column height"¹. According to Bayr and Dommenges (2013), for an "isobaric thermal expansion of the air column" it follows from the ideal gas law that

$$d\eta = \frac{\eta}{T} dT, \quad (2)$$

where T is temperature. Bayr and Dommenges (2013) propose that "to balance the heights of the two columns at the end, half of the height difference is moved from the warmer to the colder air volume". They conclude that using Eqs. (1) and (2) one obtains how SLP depends on temperature

$$\frac{dp}{dT} = \frac{1}{2} \rho g \frac{\eta}{T}. \quad (3)$$

We first note that the resulting equation (3), which forms the basis for all analyses presented by Bayr and Dommenges (2013), mathematically contradicts the preceding equations (1) and (2) from which it presumably derives. Indeed, combining (1) and (2) we find that the minus sign in (3) has been lost, while the 1/2 multiplier has been added (cf. Eq. (17) below).

The physical validity of the derivation (1)-(3) is further undermined by the use of the incorrect hydrostatic equation (1) and by the lack of an explicit definition of the key variables. For atmospheric air conforming to the ideal gas law

$$p = NRT, \quad R = 8.3 \text{ J mol}^{-1} \text{ K}^{-1}, \quad (4)$$

where N is molar density, the correct hydrostatic equilibrium equation is

$$dp(z) = -\rho(z)g dz, \quad \frac{\partial p}{\partial z} = -\frac{p}{h}, \quad h \equiv \frac{RT}{Mg}, \quad (5)$$

where M is molar mass. Here z is not the "air column height", but an arbitrary height in the atmosphere, $dp(z)$ is not the change of SLP with time, but the spatial change of air pressure over a small vertical distance dz at height z . Note that the exponential scale height h of pressure conforms to (2) but not to (1).

The "air column height" η is never formally defined by Bayr and Dommenges (2013) despite balancing this particular height is key to their model. To estimate dp/dT from (3) Bayr and Dommenges (2013) set ρ in (3) equal to the mean air density in the troposphere $\rho = \rho_a = 0.562 \text{ kg m}^{-3}$. They take η equal to the height H of the tropical troposphere

¹In the derivation of Bayr and Dommenges (2013) η in (1) is denoted as h .

$\eta = H = 16.5$ km and temperature T equal to the mean tropospheric temperature T_a defined as the mean air temperature below 100 hPa, $T = T_a = 263.6$ K. Then (3) gives $dp/dT = 1.7$ hPa K⁻¹.

Density ρ in (3) and (1) is not well defined either as it is not specified to which part of the atmospheric column it pertains. While air temperature $T(z)$ varies by about 30% at most from its surface value to the top of the troposphere, tropospheric air density $\rho(z)$ as well as air pressure $p(z)$ vary by an order of magnitude. In their quantitative estimate Bayr and Dommenget (2013) interpreted dp as describing *sea level* pressure change but for density ρ they took the *mean tropospheric* instead of surface value. This choice was incorrect as we demonstrate below (see Eq. (17) in the next section).

3 Isobaric height

The model of Bayr and Dommenget (2013) did not consider how temperature might vary with height. We will here derive a general relationship linking surface pressure and temperature to the vertical structure of the atmosphere. We will allow air temperature to vary with height with a lapse rate $\Gamma \equiv -\partial T/\partial z$, which is independent of height but can vary in the horizontal direction.

We introduce the following dimensionless variables to replace height z and lapse rate Γ :

$$Z \equiv \frac{z}{h_s}, \quad c \equiv \frac{\Gamma}{\Gamma_g}, \quad h_s \equiv \frac{RT_s}{Mg} \equiv \frac{T_s}{\Gamma_g}, \quad \Gamma_g \equiv \frac{Mg}{R} = 34 \text{ K km}^{-1}, \quad M = 29 \text{ g mol}^{-1}. \quad (6)$$

For air temperature we have

$$T(Z) = T_s(1 - cZ), \quad Z < c^{-1}, \quad T_s \equiv T(0). \quad (7)$$

The hydrostatic equilibrium equation (5) assumes the form

$$-\frac{\partial p}{\partial Z} = \rho g h_s = \frac{p}{1 - cZ}. \quad (8)$$

Solving (8) for $p \geq 0$ we have

$$\ln \frac{p}{p_s} = - \int_0^Z \frac{dZ'}{1 - cZ'} = \frac{1}{c} \ln(1 - cZ) \approx -Z - \frac{1}{2}cZ^2. \quad (9)$$

The approximate equality in (9) holds for $cZ \ll 1$, which corresponds to $z \ll h_s(\Gamma_g/\Gamma) = 45$ km, which is always the case in the troposphere.

Pressure $p(z)$ and temperature $T(z)$ at a given height z are functions of p_s , T_s and Γ . Taking the total differential of the approximate relationship for p (9) over these three variables we obtain:

$$dp = p_s(da + Zdb - \frac{1}{2}Z^2dc)e^{-Z}, \quad (10)$$

where da , db and dc stand for the dimensionless differentials of p_s , T_s and Γ :

$$da \equiv \frac{dp_s}{p_s} \approx \frac{dp_s}{\bar{p}_s}, \quad db \equiv \frac{dT_s}{T_s} \approx \frac{dT_s}{\bar{T}_s}, \quad dc \equiv \frac{d\Gamma}{\Gamma_g}, \quad (11)$$

where $\bar{p}_s = 1013$ hPa is the annual mean SLP, $\bar{T}_s = 298$ K is the annual mean surface air temperature in the tropics. With height z fixed, these differentials describe the change of respective variables in time and/or horizontal dimension. The inaccuracy of the approximate relationships in (11) is determined by the relative changes of SLP and surface temperature across the tropics. For the zonally averaged p_s and T_s this inaccuracy does not exceed 4%.

Isobaric height $z_e \equiv Z_e h_s$ is defined from (10) as the height where $dp = 0$. It is determined from the following quadratic equation:

$$da + Z_e db - \frac{1}{2} Z_e^2 dc = 0, \quad Z_e = \frac{db}{dc} \left(1 \pm \sqrt{1 + 2 \frac{da}{db} \frac{dc}{db}} \right). \quad (12)$$

There are at maximum two isobaric heights. Note that the isobaric height Z_e (12) does not depend on lapse rate c but only on its differential dc . This is a consequence of the smallness of $cZ \ll 1$ in the troposphere.

When $db = 0$, i.e., when the surface temperature does not vary, but only lapse rate does, we have from (12)

$$\frac{da}{dc} = \frac{Z_e^2}{2}. \quad (13)$$

The surface pressure change is proportional to the change in lapse rate, i.e. the pressure is lower where the lapse rate is smaller, with the proportionality coefficient equal to half the squared isobaric height.

By analogy with the isobaric height, isothermal height $z_i \equiv Z_i h_s$ is found by taking total differential of T (7) over T_s and Γ and putting $dT = dT_s - T_s Z_i dc = 0$. This gives

$$Z_i = \frac{db}{dc} = \frac{1}{h_s} \frac{dT_s}{d\Gamma}, \quad z_i \equiv Z_i h_s = \frac{dT_s}{d\Gamma}. \quad (14)$$

From (12) and (14) we obtain the following relationship for the ratio of the differentials of surface pressure and temperature (11):

$$\frac{da}{db} = -Z_e \left(1 - \frac{1}{2} \frac{Z_e}{Z_i} \right). \quad (15)$$

When, as in the model of Bayr and Dommenges (2013), lapse rate is assumed to be constant with $dc = 0$, we have $Z_i = \infty$ and (15) becomes (cf. 13)

$$\frac{da}{db} = -Z_e. \quad (16)$$

Expressing this result using notations (11) we find

$$\frac{dp_s}{dT_s} = -\frac{z_e}{h_s} \frac{p_s}{T_s} = -\rho_s g \frac{z_e}{T_s}. \quad (17)$$

Comparing (17) to (3) of Bayr and Dommenges (2013) we notice the absence of coefficient $1/2$ in (17) and the presence of surface air density ρ_s in (17) instead of an undefined air density ρ in (3). If, as did Bayr and Dommenges (2013), one assumes z_e to be equal to the tropospheric height $H = 16.5$ km, then Eq. (17) with $\rho_s = 1.2$ kg m⁻³ and $T_s = 300$ K yields $dp_s/dT_s = -6.5$ hPa K⁻¹. This estimate is 2.7 times greater by absolute magnitude than the ratio $dp_s/dT_a = -2.4$ hPa K⁻¹ obtained by Bayr and Dommenges (2013, their Fig. 2) from observations (note that in the case considered in the model of Bayr and Dommenges (2013) with $dc = 0$ we have $dT_s/dT_a = T_s/T_a \approx 1$ and $dp_s/dT_a \approx dp_s/dT_s$, see Appendix A). This discrepancy shows that neither the tropospheric height nor the mean tropospheric density determine the ratio of pressure and temperature changes in the tropical atmosphere.

In the general case the ratio $da/db = (dp_s/dT_s)(T_s/p_s)$ (15) is controlled not only by the isobaric height Z_e but also by the isothermal height Z_i . Ratios da/db and db/dc in (12) and (14) can be understood as the ratios of the gradients of the corresponding variables, e.g. $da/db = (\partial p_s/\partial y)/(\partial T_s/\partial y)(T_s/p_s)$, where $(\partial p_s/\partial y)/(\partial T_s/\partial y)$ is the ratio of pressure and temperature gradients in a given y direction (e.g. along the meridian). In this case for any y the value of z_e (or z_i) has the meaning of a height where $\partial p/\partial y = 0$ (or $\partial T/\partial y = 0$),

i.e. where pressure (or air temperature) does not vary over y . Second, for a particular grid point these ratios can be understood as the ratio of temporal derivatives: $dp_s/dT_s = (\partial p_s/\partial t)/(\partial T_s/\partial t)$. In this case z_e and z_i represent the height of a pressure level and a temperature level that do not change with time. Finally, these ratios can be understood as the ratios of small finite differences between pressure or temperature in a given grid point and a certain reference value of pressure or temperature, $dp_s/dT_s = \Delta p_s/\Delta T_s$.

In all these cases the proportionality between pressure and temperature variations, either temporal or spatial, will result if z_e and z_i are constant, see (15). We can estimate all parameters in (15) from empirical data to see if such a relationship holds across the tropics.

4 Data analysis

We used NCAR-NCEP reanalysis data on SLP and surface air temperature, as well as on geopotential height and air temperature at 13 pressure levels provided by the NOAA/OAR/ESRL PSD, Boulder, Colorado, USA, from their Web site at <http://www.esrl.noaa.gov/psd/> (Kalnay et al., 1996). As an estimate of the mean tropospheric temperature we took TTT (Temperature Total Troposphere) MSU/AMSU satellite data provided by the Remote Sensing Systems from their Web site at <http://www.remss.com/measurements/upper-air-temperature> (Mears and Wentz, 2009). Monthly values of all variables were averaged over the time period from 1978 (the starting year for the TTT data) to 2013 to obtain 12 mean monthly values and one annual mean for each variable for each grid point on a regular $2.5^\circ \times 2.5^\circ$ global grid.²

All variables were zonally averaged. Meridional gradients $\partial X/\partial y$ of variable X ($X = p_s, T_s$) at latitude y were determined as the difference in X values at two neighboring latitudes and dividing by 2.5° : $\partial X(y)/\partial y \equiv [X(y + 1.25^\circ) - X(y - 1.25^\circ)]/2.5^\circ$. Meridional pressure gradients corresponding to pressure level p_j were calculated from the geopotential height gradient $\partial p_j/\partial y = (\partial z_j/\partial y)p_j/h_j$, where z_j is the geopotential height of pressure level p_j , $h_j = RT_j/(Mg)$ is the exponential pressure scale height (5) and T_j is air temperature at this level. The following pressure levels covering the tropical troposphere were considered: 1000, 925, 850, 700, 600, 500, 400, 300, 250, 200, 150, 100 and 70 hPa. Isobaric height z_e at each latitude was determined as the minimal height where the meridional pressure gradient changes its sign.

In Fig. 1 we plotted the observed isobaric height z_e and compared it with the observed ratio of the meridional gradients of SLP and surface air temperature $-h_s(da/db) \equiv -h_s(dp_s/dT_s)(T_s/p_s) = -h_s(\partial p_s/\partial y)/(\partial T_s/\partial y)(T_s/p_s)$. There are two take-away messages from Fig. 1. First, the isobaric height of the tropical atmosphere is not constant: it rises steeply from zero at the outer borders of Hadley cells to above the top of the troposphere near the equator. During some months (e.g., June, July, August) it also has a trough at the equator. Second, the isobaric height does not universally determine the local ratio between surface gradients of pressure and temperature as illustrated by the discrepancy between the purple and black curves. The two curves have a tendency to match at low and depart from one another at high values of empirical z_e . The observed meridional variation of z_e is associated with the variation in the direction of geostrophic zonal winds. Since the velocity of these winds is proportional to the meridional pressure gradient, at $z = z_e$ they

²TTT data array contains 144 (360/2.5) longitude and 72 (180/2.5) latitude values each pertaining to the center of the corresponding grid point. NCAR-NCEP data arrays contain 144 longitude and 73 latitude values each pertaining to the border of the corresponding grid point. E.g., the northernmost latitude in the NCAR-NCEP data is 90°N , while for the TTT data it is $90 - 2.5/2 = 88.75^\circ\text{N}$. This discrepancy was formally resolved by adding an empty line to the end of the TTT data such that the number of lines match and matching i, j grid points in the two arrays. In the result, every TTT value refers to a point in space that is 1.25 degree to the South and to the East from the coordinate of the corresponding NCAR-NCEP value. This relatively small discrepancy did not appear to have any impact on any of the resulting quantitative conclusions (i.e. if instead one moves TTT points to the North, the results are unchanged).

have zero velocity. The surface $z = z_e$ is the surface where zonal winds change their direction (cf. Fig. 1a of Schneider, 2006). Beneath this roof-like surface (with slopes in the two hemispheres) the pressure falls towards the equator and the zonal winds blow from East to West.

To estimate the observed da/db ratio from (15) we need to know the isothermal height Z_i . In their model Lindzen and Nigam (1987) adopted a constant isothermal height equal to 10 km. They observed that the horizontal temperature differences at the level of $z_{LN} = 3$ km are 30% smaller than the corresponding differences at the sea level: $\Delta T(z_{LN}) = 0.7\Delta T_s$. From $T(z_{LN}) = T_s - \Gamma z_{LN}$ and (14) we obtain $z_i \equiv \Delta T_s / \Delta \Gamma = z_{LN} / 0.3 = 10$ km. This estimate is in approximate agreement with observations of the zonally averaged temperature gradient: the isothermal height in the tropical atmosphere corresponds to the pressure level of 200 hPa or about 12 km (Fig. 2). The blue curve in Fig. 1 shows that Eq. (15) describes the observed da/db ratio better than Eq. (16) (black curve) (note that in the regions where $db \approx 0$ and da/db apparently cannot be estimated from the data with sufficient accuracy).

Taking a derivative of $-da/db$ (15) over latitude y at constant Z_i

$$\frac{\partial}{\partial y} \left(-\frac{da}{db} \right) = \frac{\partial Z_e}{\partial y} \left(1 - \frac{Z_e}{Z_i} \right) \quad (18)$$

reveals that the $-da/db$ ratio has an extremum (maximum) for $Z_e = Z_i$, i.e. where the isobaric height z_e approaches 12 km. With Z_e growing beyond Z_i ($\partial Z_e / \partial y > 0$, $Z_e > Z_i$), the derivative changes its sign and $-da/db$ starts to decline. As the term in brackets in (18) is less than unity, the meridional variation of $-da/db$ ratio is always less than that of the isobaric height Z_e . When Z_e reaches twice the isothermal height, $Z_e \rightarrow 2Z_i$, from (15) we have $-da/db \rightarrow 0$. This is a point of singularity, with $da = db = dc = 0$ and pressure coinciding between the considered equatorial columns at all heights, including $z = 0$ and $z = z_i$ (see the green line in Fig. 4e,h below).

This equatorial minimum of $-da/db$ is relevant to the problem of "back pressure" in the model of Lindzen and Nigam (1987). Lindzen and Nigam (1987) proposed that pressure differences are negligible along height $z_{LN} = 3$ km which corresponds to pressure level of 700 hPa. The $-da/db$ ratio corresponds to this height around the 20th latitudes where the absolute magnitude of the pressure gradient is the largest (Fig. 1). At lower latitudes it grows to about five kilometers to decline to near zero in the immediate vicinity of the equator in some months. If $-da/db$ ratio is assumed to be a constant corresponding to $z_e = 3$ km, this leads to an overestimate of the pressure gradient near the equator and an overestimate of the equatorial moisture convergence. To cope with this problem Lindzen and Nigam (1987) introduced a "back pressure" correction to their model which adjusted the near-equatorial pressure field to fit the observations. However, we can see from Fig. 1 that the concept of a constant isobaric height linking surface pressure and temperature does not hold at large in the tropics. In particular, the assumption of Lindzen and Nigam (1987, their Eq. 9a) that the latitudinal variation in z_e (or $-da/db$) is small apparently does not hold³.

³We make a brief comment on an atmosphere where as in the model of Lindzen and Nigam (1987) the isobaric height would be constant. How would winds depend on z_e in such an atmosphere? A small isobaric height at fixed surface temperature gradients means that the surface pressure gradients are small. In the limit $z_e \rightarrow 0$ the surface pressure gradients disappears and the low-level winds should vanish. Contrary to this expectation Lindzen and Nigam (1987) found little dependence of meridional winds on z_e in their model. A smaller z_e expectedly produced weaker surface pressure gradients, but it also produced a proportionally larger damping coefficient $\epsilon \equiv C_D |V_c| / z_e$, where C_D is a constant and V_c is a typical wind speed at z_e taken by Lindzen and Nigam (1987) to be equal to 8 m s^{-1} . As a result of a weaker meridional pressure gradient, zonal wind did decrease proportionally to the surface pressure gradient. However, the meridional wind proportional to the product of zonal wind and the damping coefficient ϵ (Lindzen and Nigam, 1987, see their Eq. 12a), did not change much. The decrease in pressure gradient was offset by an increase in the damping coefficient ϵ , such that the low-level air convergence remained approximately independent of z_e . However, this conclusion critically derives from the assumed constancy of V_c — characteristic wind speed

Another illustration to the same problem is provided by the results of Bayr and Dommenges (2013). Bayr and Dommenges (2013, their Fig. 2) made a regression of spatial SLP differences $\Delta p_s \equiv p_s - \bar{p}_s$ versus mean tropospheric temperature differences $\Delta T_a \equiv T_a - \bar{T}_a$, where p_s and T_a are values in a given gridpoint and \bar{p}_s and \bar{T}_a are the mean tropical values⁴. By construction, this regression line goes through the axis origin ($\Delta p_s = 0$, $\Delta T_a = 0$). The regression slope of $\Delta p_s/\Delta T_a = -2.4$ hPa K⁻¹ obtained by Bayr and Dommenges (2013) corresponds to $\Delta p_s/\Delta T_s \approx -1.3$ hPa K⁻¹ (see Appendix A on the relationship between the mean tropospheric temperature T_a and surface temperature T_s). From (17) for $T_s = 298$ K, $p_s = 1013$ hPa and $h_s = 8.7$ km (6) and $\Delta p_s/\Delta T_s = -1.3$ hPa K⁻¹ we obtain an average $z_e = 3$ km in agreement with the assumption of Lindzen and Nigam (1987). However, as the linear regression minimizes the departure of the empirical points from the theoretical curve, the slope of a regression line that goes through the axes origin is set by the values that depart most from the zero point. The smaller Δp_s and ΔT_s values make the least contribution to the determination of the regression slope. Therefore, the regression made by Bayr and Dommenges (2013) does not actually estimate the pantropical mean value of the ratio between pressure and temperature variations. Rather, the regression slope characterizes the value of this ratio where Δp_s and ΔT_s are the largest.

Our own analysis of the seasonal dynamics of the relationship between pressure and temperature confirms the absence of a universal ratio between pressure and temperature changes. For each grid point, we made a reduced major axis regression of the monthly changes of pressure $\tilde{\Delta p}_s$ on the monthly changes of temperature $\tilde{\Delta T}_s$. Here $\tilde{\Delta p}_s \equiv p_s(m_2) - p_s(m_1)$ and $\tilde{\Delta T}_s \equiv T_s(m_2) - T_s(m_1)$, where m_1 and m_2 are two consecutive months (e.g., December and January). A similar analysis was performed for p_s and T_a .

In the equatorial land regions with high rainfall — in the Amazon and Congo river basins, see point C in Fig. 3 — the regressions were not significant at 0.01 probability level⁵. Where the regressions are significant, the largest (by absolute magnitude) regression slopes tend to be concentrated in the regions of the largest SLP gradients, i.e. around the 15–20th latitudes (Fig. 3). These local dependences between $\tilde{\Delta p}_s$ and $\tilde{\Delta T}_s$ can be explained by the seasonal migration of the Hadley cells where lower pressure is spatially associated with higher temperature (see Fig. 8b below). This explanation is supported by the fact that the tropical mean of the local $\tilde{\Delta p}_s/\tilde{\Delta T}_s$ ratio, -1.1 hPa K⁻¹ (Fig. 3), is approximately equal to the tropical mean ratio of the spatial differences $\Delta p_s/\Delta T_s = -1.3$ hPa K⁻¹ (see

at the top of the boundary layer. In reality V_c is not independent of z_e . In the model of Lindzen and Nigam (1987) the boundary layer height was assumed to be equal to $z_e \sim 3$ km, which is unrealistic. In the real atmosphere the height of boundary layer h_b is much smaller, $h_b \sim 1$ km $\ll z_e$. Because of this, pressure gradients at the top of the boundary layer are determined by the surface pressure gradients and close to them. Since at the top of the boundary layer winds are approximately geostrophic (Back and Bretherton, 2009), this means that the geostrophic wind speed V_c at the top of the boundary layer (which is used in the determination of the damping coefficient) is approximately proportional to the surface pressure gradient. Consequently, it decreases with decreasing z_e . In the result, with decreasing z_e (decreasing surface pressure gradient), surface winds will decline as well proportionally to the declining V_c .

⁴Note that Fig. 2 of Bayr and Dommenges (2013) describes the relationship between spatial differences of pressure and temperature rather than between their temporal changes. In that figure Δp_s and ΔT_a values from the four seasons are plotted together. It is clear that if there were no seasonal change of $\Delta p_s/\Delta T_a$ whatsoever, such a regression would nevertheless produce a non-zero slope reflecting the time-invariable spatial association between higher temperature and lower pressure.

⁵On land, sea level pressure is not an empirically measured variable, but is calculated from pressure $p_l(z_l)$, temperature $T_l(z_l)$ and the geopotential height z_l of the land surface assuming $\Gamma = 6.5$ K km⁻¹ for $0 \leq z \leq z_l$, where $z = 0$ corresponds to the sea level. This definition introduces a formal dependence of p_{sl} (sea level pressure on land) on surface air temperature T_l , the strength of which is directly proportional to z_l . That is, p_{sl} diminishes with growing T_l even if p_l and, hence, the amount of gas in the atmospheric column remains constant. Approximating the hydrostatic equation (5) as $(p_l - p_{sl})/z_l = -p_l/h$, $h = RT_l/(Mg)$, and taking the derivative of this equation over T_l at constant p_l we obtain $dp_{sl}/dT_l = (z_l/h)p_l/T_l$. For the mean geopotential height $z_l = 0.6$ km of the tropical land, $p_l = 950$ hPa and $T_l = 295$ K we find $dp_{sl}/dT_l = -0.2$ hPa K⁻¹, i.e. about 20% of the mean ratio established by us for the tropical land (Fig. 3) is not related to any air redistribution but is a formal consequence of the definition of p_{sl} .

Appendix A). Likewise the result of Bayr and Dommenget (2013, cf. their Figs. 2 and 8) — that the long-term trends in p_s and T_a have a similar ratio -2.4 hPa K^{-1} as their mean spatial differences — indicates that these trends reflect a shift in the form (e.g., widening) or displacement of the Hadley cells.

Outside the tropics where, in contrast to the tropics, areas of low pressure are at the same time areas of low temperature (particularly the southern Ferrel cell), the seasonal relationship between pressure and temperature changes is generally less consistent than it is in the tropics and somewhere it is reversed — i.e., pressure and temperature rise or decline together (see point E in Fig. 3).

Since the relationship between tropical pressure and temperature is apparently variable, a model that assumes a constant ratio between temporal changes of pressure and temperature cannot be used for predicting regional changes of pressure from changes in temperature in a warming or cooling climate. Nor can a model based on a constant ratio between spatial differences of temperature and pressure successfully describe the time-averaged circulation. Relative errors resulting from such models will be the largest where the pressure and temperature variation are the smallest by absolute magnitude. Lindzen and Nigam (1987) emphasized how a distorted representation of the small pressure gradients in the equatorial regions can mislead model-derived estimates of circulation and moisture convergence intensity.

5 Vertical profiles of pressure differences

We will now discuss in a broader context the question of causality: is there a physical mechanism by which differential heating at the surface could cause a surface pressure gradient?

In this section we will consider differentials in (11) as corresponding to small finite differences in respective variables (Δp , ΔT and $\Delta \Gamma$) between two air columns that are separated along the meridian by a small finite distance Δy . Then $dp = \Delta p(z)$ in (10) is a small pressure difference at a given height between the two air columns. This difference has an extremum above the isobaric height Z_e (12) at a certain height Z_0 which is determined by taking the derivative of (10) over Z and equating it to zero, see (10), (12) and (14):

$$\frac{\partial \Delta p}{\partial Z} = 0, \quad da + Z_0 db - \frac{1}{2} Z_0^2 dc - db + Z_0 dc = 0, \quad Z_0 = 1 + Z_i \pm \sqrt{(Z_e - Z_i)^2 + 1}. \quad (19)$$

At this height the pressure difference is equal to

$$\Delta p_0 \equiv \Delta p(Z_0) = p_s e^{-Z_0} \left(da + Z_0 db - \frac{1}{2} Z_0^2 dc \right) = p_s e^{-Z_0} (db - Z_0 dc). \quad (20)$$

Note that by definition when $\Delta p_0 = 0$ we have $Z_e = Z_0 = Z_i$. As is clear from Fig. 4, where the vertical profiles of $\Delta p(z)$ (10) are shown for different values of da , db and dc , this extremum corresponds to the maximum pressure difference between the air columns above the lower isobaric height.

When the vertical lapse rate is constant, $dc = 0$, from (19) we have $Z_0 = 1 - da/db$. In this case, as is clear from (20), for small values of $da/db \ll 1$ the magnitude of Δp_0 does not depend on da , but is directly proportional to db , i.e. to ΔT_s (11) (Fig. 4a). This means that under these particular conditions a surface temperature gradient directly determines the pressure gradient *in the upper atmosphere*. In this sense there is no difference between surface temperature gradient and a gradient of lapse rate related to latent heat release — both can only determine a pressure surplus aloft, cf. Fig. 4a,b and Eqs. (15) and (13). We emphasize that while the magnitude of the tropospheric pressure gradient can be approximately specified from considerations of the hydrostatic balance and surface temperature gradients alone, the magnitude of the surface pressure gradient cannot.

In the general case, the height of the extremum Z_0 as well as the ratio between the pressure surplus aloft and the pressure shortage at the surface $\Delta p_0/\Delta p_s$ are functions of two parameters, the isobaric and isothermal heights Z_i and Z_e . Thus, when Z_i and Z_e are constant in space or time, the ratio between the pressure surplus aloft and the pressure shortage at the surface in the warmer column is constant as well: the larger the pressure surplus aloft, the larger the surface pressure shortage, with a direct proportionality between the two. This is consistent with the conventional thinking about differential heating, that the upper pressure surplus will cause air to diverge from the warmer column, the total amount of gas will diminish and there appears a shortage of pressure at the surface $\Delta p_s < 0$.

This reasoning would be testable if it were possible to specify Z_i and Z_e independently of the da/db ratio. However, such an independent specification apparently does not exist, while Z_e varies significantly in space and time (Figs. 1, 2). The ratio between the surface pressure gradient and the maximum pressure gradient in the upper atmosphere

$$\frac{\partial p_s/\partial y}{\partial p_0/\partial y} = -e^{Z_0} \frac{Z_e [1 - Z_e/(2Z_i)]}{1 - Z_0/Z_i} \quad (21)$$

also varies within broad margins (Fig. 5). It is larger at the equator than at the poleward ends of the cell: the larger the pressure gradient aloft by absolute magnitude, the smaller, in relative terms, the pressure gradient at the surface (Fig. 5).

Our reading of current evidence and arguments is that a physical theory explaining how differential heating determines low-level pressure gradients does not exist. That is to say, it remains impossible to link observed pressure gradients to gradients of air temperature using fundamental atmospheric constants and physical relationships. Thus, any air circulation model attempting to reproduce low-level circulation based on differential heating physics must tune its key parameters (e.g., the da/db ratio) to fit with observations. Such a fitted model cannot readily be used to test the underlying relationships as their validity has already been assumed. We propose that surface pressure and temperature gradients are generated primarily by water vapor dynamics. We will now explain the physical mechanisms.

6 Condensation-induced pressure differences

The key physical proposition is that water vapor condensation in the moving air releases potential energy at a rate s (W m^{-3}) proportional to air velocity in the direction of decreasing partial pressure of water vapor p_v (Makarieva and Gorshkov, 2010; Makarieva et al., 2013b, 2014a):

$$s = -p\mathbf{w}\nabla\gamma - \mathbf{v}\nabla p_v, \quad \gamma \equiv p_v/p. \quad (22)$$

We consider zonally averaged stationary circulation where all variables depend on height z and distance along the meridian y ; \mathbf{w} and \mathbf{v} are the vertical and horizontal (meridional) air velocities, respectively. The first term describes condensation in the rising air. The second term describes condensation or evaporation in the air moving along a horizontal temperature gradient. Integrating s over height in the entire atmosphere yields precipitation P per unit area of the Earth's surface in energy units PRT (W m^{-2}). With potential energy from condensation converted to the kinetic energy of atmospheric air, PRT should be equal to the independently estimated total power of atmospheric circulation on Earth. This agrees well with observations (Makarieva et al., 2013b,a).

In hydrostatic equilibrium the kinetic power is generated by horizontal pressure gradients only (the vertical pressure gradients are offset by the gravity force). Integrating s (22) over the entire volume occupied by the condensation-induced circulation we have

$$-\int \mathbf{v}\nabla p dz dy = \int s dz dy = \int [-p\mathbf{w}\nabla\gamma - \mathbf{v}\nabla p_v] dz dy. \quad (23)$$

Eq. (23) formulates a constraint on the total kinetic power of a stationary circulation driven by condensation. Our goal is now to show that under reasonable assumptions about the geometry of the circulation and condensation areas Eq. (23) makes it possible to estimate surface pressure difference Δp_s across the circulation.

At the outer borders of our circulation $y = y_1$ and $y = y_2$ meridional velocity v is zero, $v(y_1) = v(y_2) = 0$ (Fig. 6). Water vapor evaporated in the upstream part of the circulation where the air descends is transported to the downstream part of the circulation where the air ascends and the imported water vapor condenses. Reflecting this water vapor transport it is convenient to divide the circulation area into two parts, the donor and the receiver areas, respectively. They are delimited by line $y = y_3$ where horizontal velocity v is maximum $v(y_3) = v_{max}$ (Fig. 6). For simplicity we assume the two parts to be of equal size. The length of the donor and receiver areas are respectively $L_d = y_3 - y_1$ and $L_r = y_2 - y_3$, total length $L = 2L_d = 2L_r = y_2 - y_1$ (Fig. 6).

We take into account that most part of kinetic energy is generated and dissipated in the narrow layer near the surface $z \leq h_b$ such that the first integral in (23) can be written as

$$\int \mathbf{v} \nabla p dz dy \equiv h_b \int (v_s \partial p_s / \partial y) dy, \quad (24)$$

where v_s and p_s are velocity and pressure at the surface and h_b is the effective height of this layer. The product $v \partial p / \partial y$ declines approximately linearly with increasing height up to 850 hPa (1.2 km) where it becomes about one order of magnitude smaller than it is at the surface (Fig. 7). This means that $h_b \approx 0.6$ km in (24) approximately coincides with the planetary boundary layer. We also assume that the low-level air moves from the colder donor area to the warmer receiver area, such that ∇p_v in (23) describes the gradient of water vapor partial pressure owing to surface evaporation that increases water vapor concentration in the surface layer $z \leq z_s$ where the relative humidity is less than unity, with z_s being the saturation level. Since $z_s \approx h_b$ we can approximate $\int \mathbf{v} \nabla p_v dz dy$ in (23) by $h_b \int (v_s \partial p_{vs} / \partial y) dy$. Using (24) and a linear approximation $-\nabla p = \Delta p / L$, $\nabla p_v = \Delta p_v / L$ we can re-write (23) as

$$(\Delta p + \Delta p_v) h_b \bar{v}_s = w_r L_r p \bar{\gamma}_r, \quad \bar{v}_s \equiv L^{-1} \int_{y_1}^{y_2} v dy, \quad w_r \equiv L_r^{-1} \int_{y_3}^{y_2} w(h_b) dy. \quad (25)$$

Here w_r is the mean vertical velocity at height h_b and $\bar{\gamma}_r = (\gamma_2 + \gamma_3) / 2$ is the mean relative partial pressure of water vapor at the surface in the receiver area, γ_2 and γ_3 are calculated, respectively, at y_2 and y_3 . When deriving the right-hand part of (25) from (23) we have taken into account that pw is approximately constant up to a height z_c where most water vapor has condensed and $\gamma(z_c) \ll \gamma_s$ (see Makarieva et al., 2013a, their Eq. A2). We have also assumed that $s = -\mathbf{v} \nabla p_v$ for $z \leq h_b$ (no condensation below h_b).

On the other hand, from the integral continuity equation at the border of the donor and receiver areas we have

$$h_b v_{max} = w_r L_r, \quad (26)$$

Assuming that v increases approximately linearly from $v(y_1) = 0$ to $v(y_3) = v_{max}$ and then decreases linearly to $v(y_2) = 0$ and neglecting the vertical variation in velocity in the boundary layer $z \leq h_b$ (Stevens et al., 2002) we put $\bar{v}_s / v_{max} = 1/2$. Using this ratio, the expression for $\bar{\gamma}_r$ and (26) we are able to cancel velocities and linear scales in (25) to obtain

$$\Delta p_s = p_s (\gamma_1 + \gamma_3) = p_{v1} + p_{v3}, \quad z \leq h_b. \quad (27)$$

The drop of surface pressure in our condensation vortex is equal to the sum of water vapor partial pressures at the two borders (y_1 and y_3) of the donor area (Fig. 6). Remarkably, the pressure drop does not depend on the linear size L of the circulation.

However, the main equation (23) from which (27) derives does not indicate the spatial scale of the air velocities and pressure gradients under consideration. If the considered

horizontal scale L includes many condensation-induced vortices with chaotically oriented pressure gradients, then the resulting large-scale pressure gradient and large-scale mean velocities v and w observed on scale L will be zero. How much of total potential energy released upon condensation is attributed to kinetic energy generation on a particular linear scale is determined by the horizontal transfer of water vapor on the considered scale. Indeed, if all moisture evaporated in one half of considered area is precipitated in the same half (without being transferred to the second half), then the horizontal pressure gradient across the area will be zero. If, on the other hand, a certain part R of moisture evaporated in the donor area is exported to the receiver area, then the power of air circulation generated on scale L will be $K = R/C$ of total condensation power C in the considered area.

From the mass balance equation for the water vapor we have

$$P_d = E - R, \quad P_r = E + R, \quad (28)$$

where P_d and P_r are total precipitation in the donor and receiver areas (that we assumed to be of equal size), R is the amount of water vapor imported from the donor area to the receiver area and E is evaporation assumed to be the same in both areas. Horizontal transport of water vapor diminishes precipitation in the donor area and increases it in the receiver area. Transfer coefficient K can be retrieved from the precipitation ratio r between the two areas:

$$K \equiv \frac{R}{P_r + P_d} = \frac{1}{2} \left(\frac{1-r}{1+r} \right), \quad r \equiv \frac{P_d}{P_r}. \quad (29)$$

The value of K can be viewed as describing the proportion of time and space that the circulation in the considered area takes the form shown in Fig. 6, while during the rest of time/space the horizontal pressure gradients on the considered area are zero. With an account of the transfer coefficient our theoretical estimate for the surface pressure difference on a spatial scale L becomes

$$\Delta p_s = K p_s (\gamma_1 + \gamma_3) = \left(\frac{p_{v1} + p_{v3}}{2} \right) \left(\frac{1-r}{1+r} \right). \quad (30)$$

We tested relationship (30) with the zonally averaged data for the two Hadley cells (Fig. 8). For each month we computed the zonally averaged profile of SLP and meridional velocity v at the surface. For each month we defined the Northern and Southern cell as the areas where $v > 0$ and $v < 0$, respectively, and computed the pressure difference Δp_s between the poleward and the equatorial borders of each cell. We calculated transfer coefficient K using donor/receiver precipitation ratios as in (29). We calculated the mean surface water vapor partial pressure $p_v = p\gamma$ by averaging the product of monthly mean relative humidity and saturated water vapor partial pressure corresponding to the monthly mean surface air temperature in each grid point. All estimated parameters are listed in Table 1.

In Fig. 9 we plotted the observed monthly Δp_s values versus the theoretical estimate (30) for the Northern and Southern Hadley cells. The annual mean theoretical estimates of Δp_s are within 30% of their observed values (Table 1), which can be considered a good agreement in the view of several simplifying assumptions that we have made. The theoretical and empirical Δp_s values display consistent changes throughout the year (Fig. 9). The order of magnitude of Δp_s is set by the partial pressure of water vapor p_{vs} in the donor area, which changes little throughout the year. The seasonal behavior of Δp_s is governed by the transfer coefficient K , which varies from 0.14 to 0.27 in the Southern cell and from 0.07 to 0.29 in the Northern cell. It is higher during the colder season, when the cell is also larger (Fig. 9c,d, see also Dima and Wallace, 2003, their Fig. 1). While the poleward border y_1 moves towards the equator during the colder season, the near-equatorial border y_2 spreads to the other hemisphere, such that the winter cell comprises a larger part of the precipitation peak than the summer cell (Fig. 8). This is manifested as an increase in the transfer coefficient K .

7 Moisture transport and surface air temperature

The surface temperature differences ΔT_s associated with pressure differences Δp_s are shown in Fig. 9c,d. In the tropical area, where the solar flux varies least with latitude compared to the extratropics, the horizontal transport of moisture and, hence, latent heat should play a major role in the spatial distribution of temperature. Water vapor evaporates in the donor area and condenses in the receiver area. Thus the donor area exports, and the equatorial receiver area imports, significant amounts of energy in the form of latent heat. How could this process influence surface temperature? We have a suggestion.

Consider an air parcel in the donor area that rises from the surface $z = 0$ up to a certain height z_p (Fig. 6). It starts from a surface pressure p_{s1} and surface temperature T_{s1} , its temperature varies with a lapse rate Γ_1 . The parcel travels at this height towards the equator where it descends and returns to the surface with a different lapse rate $\Gamma_2 > \Gamma_1$. A relevant example is the ascent with a moist adiabatic and descent with a dry adiabatic lapse rate. Upon the descent, at the surface this parcel will have a higher temperature $T_{s2} = T_{s1} + \Delta T_s > T_{s1}$. It will also have a lower pressure $p_{s2} = p_{s1} + \Delta p_s < p_{s1}$. This is because in the descending parcel being on average warmer than the ascending parcel, pressure grows with diminishing height more slowly (its pressure scale height h (5) is larger). Therefore, for such a process to be possible, the area where the warmer parcel descends must have a lower surface pressure than where it started its ascent. (A remarkable example of such descending motion in a warm low pressure area occurs in the eyes of the tropical storms, which are both warmer than the zone of intense convection at the windwall (Montgomery et al., 2006) and have lower pressure (Makarieva and Gorshkov, 2011).)

If pressure and temperature vary considerably less at z_p (the height at which the parcel moves) than at the surface, this height can be considered as both isobaric and isothermal, $z_p = z_e = z_i$. This condition allows one to find the difference in the parcel's temperatures at the surface from the known values of Δp_s and $\Delta \Gamma$ using (14) and (15):

$$Z_p = Z_e = Z_i = \frac{db}{dc} = -2 \frac{da}{db}, \quad db = \sqrt{-2da \, dc}, \quad \Delta T_s = T_s \sqrt{-2 \frac{\Delta p_s}{p_s} \frac{\Delta \Gamma}{\Gamma_g}}. \quad (31)$$

Taking $\Delta p_s = -7.7$ hPa for the mean difference between the inner and outer ends of the Hadley cell (Table 1) and $\Delta \Gamma = 4$ K km⁻¹ equal to the difference between the dry adiabatic lapse rate and moist adiabatic lapse rate at $T \approx 283$ K (Makarieva and Gorshkov, 2010, their Fig. 4e) with $p_s = 1013$ hPa and $T_s = 298$ K we obtain from (31) $\Delta T_s = 12.6$ K, ratio $\Delta p_s / \Delta T_s = -0.6$ hPa K⁻¹ and height $z_p \equiv Z_p h_s = 3.2$ km.

Theoretical estimate of the ratio $\Delta p_s / \Delta T_s = -0.6$ hPa K⁻¹ is smaller by absolute magnitude than the observed (the mean annual ratio is -0.9 hPa K⁻¹ for the Southern and -0.7 hPa K⁻¹ for the Northern cell), while the estimated temperature difference 12.6 K is larger than the observed ($\Delta T_s = 8.3$ K for the Southern and 9.0 K for the Northern cell). Another discrepancy between the theory and observations is that the vertical mixing apparently spreads the temperature difference well above the parcel height z_p . While there is indeed a local minimum of the temperature difference between the equator and the wider tropics $z_p \approx 3$ km (Fig. 2a-e), this height is not strictly isothermal.

On the other hand, theoretical result (31) agrees with the observations in several essential ways. First, the pressure difference between the 30th latitudes and the equator at the estimated height $z_p = 3.2$ km is close to zero and indeed much smaller than at the surface (Fig. 10), supporting our assumption that for the considered air parcel $z_p = z_e$. Note that for Eq. (31) to hold, we do not need z_p to be the local isobaric height at any point — we have only demanded that the pressure difference along z_p between the areas where the parcel ascends and where it descends is negligible compared to the pressure difference at the surface. Second, the atmospheric layer up to $z_p = 3.2$ km does indeed represent the layer where the lapse rate increases from the wider tropics to the equator (Fig. 11). It is

in this low layer that the equator, despite being the hotspot of rainfall and convection, has a steeper lapse rate than the rest of the tropics. The equatorial lapse rate becomes moist adiabatic only starting from about 5 km (Mapes, 2001). The descending motion of the low-level air parcels transporting latent heat from the donor area provides an explanation to this remarkable feature. Third, height of about 3 km represents the upper boundary of the trade wind inversion layer (Schubert et al., 1995). Shallow convective clouds forming in this layer represent a prominent feature of tropical convection — in fact they are one of the three dominant convective modes (Johnson et al., 1999). This shallow convection is more common to the poleward ends of the Hadley cells and is absent near the equator supporting the idea that the ascending motion driving the low-level convection is concentrated in that area. Thus, the existence of moist air parcels rising around the 30th latitudes up to 3 km and descending much closer to the equator does not contradict what we know about the tropical cloud cover. Horizontal transport of latent heat and its conversion to sensible heat in the lower atmosphere near the equator thus appears able to explain the observed surface temperature distributions.

8 Discussion

In the literature surface pressure gradients are discussed as *determined* or *generated* by gradients in sea surface temperature (Lindzen and Nigam, 1987; Sobel and Neelin, 2006; An, 2011). For example, Sobel and Neelin (2006, p. 324) in their discussion of the model of Lindzen and Nigam (1987) noted that surface temperature determines temperature in the atmospheric boundary layer, which, in its turn, determines surface pressure via a hydrostatic relationship. Likewise Bayr and Dommenges (2013) characterized the differential heating of the planetary surface as a driver of changes in surface pressure.

Here we have revisited the concept of differential heating in a hydrostatic atmosphere. As considered in Section 5, under certain conditions the surface temperature gradients can indeed approximately determine pressure gradients, but only in the upper atmosphere. However, the magnitude of the surface pressure gradient cannot be deduced from the magnitude of surface temperature gradient unless some additional postulates are made that would a priori specify a relationship between the two. In particular, a linear relationship between surface gradients of temperature and pressure is contingent upon the existence of a constant isobaric height where pressure does not vary. The existence of such a constant height was postulated in the models of Lindzen and Nigam (1987) and Bayr and Dommenges (2013).

Here we have used empirical evidence to demonstrate that there is neither a constant isobaric height in the tropics nor is such a constancy a reasonable zero-order approximation. The isobaric height (defined as the height where the meridional pressure gradient is zero) varies from zero at the 30th latitudes to over 16 km near the equator. Its magnitude cannot be deduced from any fundamental atmospheric parameters — the physical model of Bayr and Dommenges (2013) proposing the height of the troposphere as a universal isobaric height was not correct (Section 2). We showed that the observed ratio between surface pressure and temperature gradients defines the magnitude of the isobaric height if one more essential parameter, the isothermal height, is known (Eq. 15). We thus conclude that the existence of a relationship between surface pressure and temperature (with warm air having low pressure) is not an argument that surface pressure gradients are driven by differential heating. Conversely, the concept of differential heating based on a constant isobaric height cannot explain why the surface temperature and pressure gradients across the tropics have the magnitudes observed.

In contrast, we have demonstrated that evaporation and condensation can produce the observed SLP differences of the order of $\Delta p_s \sim 10$ hPa in the zonally averaged Hadley cells (Section 6). The scale of the pressure differences is set by the mean partial pressure of the water vapor in the donor area. Their actual magnitude depends on the efficiency K of

horizontal moisture transport (30). Coefficient K (29) describes the ratio of the intensity of condensation associated with horizontal moisture transport on a length scale comparable to the length of the Hadley cell to the intensity of condensation associated with smaller-scale local eddies. The efficiency K of horizontal moisture transport grows with the increasing linear size of the Hadley cell. In winter cells both in Northern and Southern hemispheres K reaches its maximum value of 0.3. In the smaller summer cells K falls to about 0.1 (Table 1). The maximum possible value of $K = 1/2$ would imply that all water vapor evaporated in the poleward half of the Hadley cell (the donor part) has been transported to the equatorial counterpart and precipitated there. $K = 0$ means that all evaporated moisture precipitates locally – i.e. that the characteristic transport length is much less than the cell length L . In such a case, when condensation is spatially uniform, the vapor sink obviously does not produce any large-scale pressure gradient.

What determines the seasonal changes in K ? Condensation in the rising air must, by mass conservation constraints, always involve some horizontal air motion. If we have an isothermal surface uniformly heated by the Sun convection can occur just by symmetry breaking: if the air begins to condense in one place, there will be rising motion and horizontal import of moisture to the area of condensation. Several studies, most importantly Holloway and Neelin (2010) for an equatorial island and Sharkov et al. (2012) in the context of tropical cyclones linked the probability of convective rain to the amount of water vapor in the atmospheric column. The higher the amount of water vapor, the higher the probability of (intense) convection. Any small differences in solar radiation over an otherwise uniform oceanic surface will translate into differences in the accumulated flux of evaporated water vapor. Since likelihood of rain rises sharply with columnar water vapor content (e.g., Holloway and Neelin, 2010, their Fig. 10b), the area receiving more solar flux will develop convection sooner than the area that receives less. This will lead to a drop of pressure and a horizontal transport of moisture towards the area where condensation takes place (see also discussion by Makarieva et al., 2014b). The pressure gradient generated through this process enhances horizontal motion and moisture transport which reinforces and enhances the pressure gradient itself. Therefore even a small gradient in solar radiation can in principle cause significant spatial gradients in condensation intensity. In such a case, condensation will be more spatially uniform (i.e., K will be lower) in summer than in winter cells, in agreement with observations (Table 1).

With condensation intensity depending on minor differences in local water vapor amounts, natural forests with their intense evapotranspiration can play a much larger role in determining the position of active convective zones than is generally recognized (Makarieva and Gorshkov, 2007; Makarieva et al., 2014b). For example, the on-going discussion concerning possible slow-down of the Walker circulation focuses on the relationships between sea level temperature and pressure (e.g., Tokinaga et al., 2012), while the concurrent large-scale deforestation on the Maritime Continent and the associated changes in evapotranspiration are never considered as possible drivers of the regional changes in convection.

We have additionally suggested that horizontal transport of latent heat from the outskirts of the Hadley cells (donor areas) toward their inner equatorial parts (receiver areas) can lead to formation of a horizontal surface temperature gradient (Section 7). Latent heat captured as water vapor at the 30th latitudes is transported by the converging air towards the equator. Convective eddies where the air descends dry adiabatically ensure that part of this heat is returned to the surface in sensible form. This process may partially account for the fact that the equator in the lower atmosphere (up to 850 hPa) has a steeper lapse rate than the rest of the tropics (Fig. 11).

In the extratropics latent heat release was discussed as a mechanism stabilising the upper tropospheric temperatures during winter time in the extratropics (Herman et al., 2008). In the tropics, the effects of evaporation and latent heat release have been considered extensively in the context of climate stability (Wallace, 1992; Ramanathan and Collins, 1991; Bates, 1999; Caballero, 2001; Bates, 2012). Wallace (1992) observed that evaporation

can cool the surface as the latent heat released in the upper atmosphere will be rapidly mixed in the horizontal dimension cooling the warm surface more than it warms cool surfaces. However, this cooling mechanism considers only *export* of local latent heat resulting from condensation of moisture evaporated in the region of ascent. Meanwhile, condensation in the ascending air is necessarily accompanied by *import* of moisture and, hence, latent heat from the adjacent areas to the area of ascent. If, as we proposed, this additional latent heat is released and converted to sensible heat in low-level eddies in the zone of convection, the outcome may be not a uniform temperature distribution but, rather, a creation of a surface temperature gradient. We have shown that moist air parcels in convective eddies rising to the height of the trade wind inversion and descending in the low pressure equatorial area can produce temperature gradients of magnitudes close to the observed.

Since higher temperatures are associated with higher atmospheric content of water vapor, a surface temperature gradient can be another mechanism responsible for the spatial non-uniformity of condensation intensity besides the surface gradient in absorbed solar radiation. If horizontal transport of latent heat is a major factor determining the surface temperature gradients in the tropics, this can provide an alternative explanation for the relative constancy of near equatorial temperatures (Wallace, 1992). Suppose the extratropics cooled compared to the equator. This enhanced the temperature difference between the equator and the tropics and led to an extra import of latent heat towards the equator. In the result, in the new cooler climate the equator cooled less than the tropics because of this extra heat. Conversely if the extratropics warm, this leads to a decline in latent heat transport towards the equator, such that in the new warmer climate the equator warms less. In the result equatorial temperatures become more stable than at higher latitudes with respect to temperature fluctuations originating in the extratropics. In summary, we believe that the perspectives opened by the concept of condensation-driven winds merit further investigations.

A Appendix: Relationship between T_s and T_a

The relationship between surface temperature T_s and the mean temperature $T_a(Z)$ of the atmospheric column below Z can be derived from (7) and the hydrostatic equation (5):

$$T_a(Z) \equiv \frac{\int_0^Z T(Z) \rho dZ}{\int_0^Z \rho dZ} = \frac{T_s}{1+c} \frac{1 - e^{-cZ} e^{-Z} e^{-cZ^2/2}}{1 - e^{-Z} e^{-cZ^2/2}}, \quad Z \equiv \frac{z}{h_s}, \quad cZ \ll 1. \quad (31)$$

Expanding (A) over c and keeping the linear term we have

$$T_a = T_s \left[1 - c \left(1 - \frac{Z}{e^Z - 1} \right) \right]. \quad (31)$$

Taking the derivative of (A) over T_s and c we obtain:

$$dc = \frac{db - dn}{1 - Z/(e^Z - 1)}, \quad dn \equiv \frac{dT_a}{T_a}. \quad (31)$$

For the height of the tropical troposphere $z = H = 16.5$ km, $T_s = 298$ K and $\Gamma = 6.0$ K km⁻¹ (Fig. 11) we have $Z = 1.9$, $c = 0.18$, $1 - Z/(e^Z - 1) = 0.66$ and obtain from (A) and (A)

$$T_a = 0.88T_s, \quad db = dn + 0.66dc, \quad \frac{dT_s}{dT_a} = \frac{1}{0.88} \left(1 + 0.66 \frac{d\Gamma}{dT_a} \frac{T_a}{\Gamma_g} \right). \quad (31)$$

The mean tropospheric $\overline{T_a} = 262$ K in the tropics estimated from (A) agrees with the tropical mean $\overline{T_a} = 261$ K that we estimate from the TTT data of Mears and Wentz (2009) and with $\overline{T_a} = 263.6$ K cited by Bayr and Dommenget (2013).

From (A) we can see that the relative changes db and dn of T_s and T_a coincide, $db = dn$, if only the lapse rate does not vary, $dc = 0$. In the tropical atmosphere this is not the case: areas with higher T_s ($db > 0$) have a higher lapse rate $dc > 0$ (Fig. 11). Therefore, in the tropics $db > dn$. Table 2 lists the results of the reduced major axis regression of $\Delta T_s = T_s - \overline{T_s}$ on $\Delta T_a = T_a - \overline{T_a}$ in the tropics (from 27.5°S to 27.5°N) for different months on land and in the ocean. On average we have $\Delta T_s / \Delta T_a = 1.8$. Therefore, the result of Bayr and Dommenget (2013) $\Delta p_s / \Delta T_a = -2.4 \text{ hPa K}^{-1}$ corresponds to $\Delta p_s / \Delta T_s = (\Delta p_s / \Delta T_a) / (\Delta T_s / \Delta T_a) = -1.3 \text{ hPa K}^{-1}$ as considered in Section 4.

B Tables

Table 1: Parameters of Eq. (30) and other relevant parameters of Hadley cells: y_1 and y_2 are the outer borders of the donor and receiver areas (Fig. 6), respectively; L cell length, P , P_d and P_r are mean precipitation in the cell as a whole, in the donor and receiver areas, respectively; K is the moisture transport coefficient (29); p_{v1} and p_{v3} are partial pressures of water vapor at the surface at y_1 and $y_3 \equiv (y_2 + y_1)/2$ (the inner border of the donor and receiver areas); p_{s1} , T_{s1} , T_{a1} are surface pressure, surface air temperature and mean tropospheric temperature, respectively, at y_1 ; Δp_s , ΔT_s and ΔT_a are differences in respective variables at y_1 and y_2 (e.g., $\Delta p_s = p_{s2} - p_{s1}$); Δp_{s*} is the theoretical estimate (30) of Δp_s .

Time	y_1	y_2	L	P	P_d	P_a	K	p_{v1}	p_{v3}	p_{s1}	T_{s1}	T_{a1}	Δp_{s0}	Δp_{s*}	ΔT_s	ΔT_a
	°lat			mm day ⁻¹				hPa			K		hPa		K	
<i>Southern cell</i>																
Jan	-35.0	-5.0	30.0	3.8	2.4	5.0	0.17	17.4	24.0	1017.0	292.3	256.9	-6.67	-7.18	6.3	5.5
Feb	-37.5	-5.0	32.5	3.9	2.6	5.3	0.18	16.5	24.7	1017.5	291.2	256.1	-7.16	-7.26	7.7	6.4
Mar	-37.5	-2.5	35.0	3.9	2.6	4.8	0.15	15.9	24.2	1018.0	290.6	255.1	-7.77	-5.90	8.5	7.6
Apr	-35.0	2.5	37.5	3.8	2.6	4.6	0.14	15.9	24.0	1018.5	290.8	254.4	-8.30	-5.60	8.7	8.5
May	-30.0	7.5	37.5	3.7	2.2	4.9	0.19	15.8	24.9	1018.7	291.1	255.0	-8.10	-7.63	8.5	7.9
Jun	-27.5	15.0	42.5	3.6	1.9	5.4	0.24	15.2	26.4	1019.8	290.5	255.3	-9.08	-10.10	10.0	7.7
Jul	-27.5	17.5	45.0	3.6	1.7	5.2	0.25	14.2	25.3	1020.8	289.7	254.9	-10.10	-9.89	10.9	7.9
Aug	-30.0	17.5	47.5	3.4	1.4	4.9	0.27	13.1	24.0	1020.9	288.6	253.5	-10.40	-9.87	12.0	9.4
Sep	-30.0	15.0	45.0	3.3	1.5	4.9	0.26	13.4	24.5	1020.3	289.3	254.0	-9.57	-9.97	10.9	8.6
Oct	-32.5	10.0	42.5	3.2	1.8	4.5	0.22	13.6	24.6	1019.5	289.1	253.6	-8.59	-8.34	10.2	8.7
Nov	-32.5	5.0	37.5	3.1	2.1	3.9	0.15	15.0	23.4	1018.0	290.7	255.0	-7.49	-5.70	8.1	7.5
Dec	-35.0	0.0	35.0	3.5	2.4	4.4	0.15	15.8	23.8	1017.0	290.8	255.4	-6.64	-6.02	7.6	7.1
Ann	-32.5	5.0	37.5	3.3	2.2	4.0	0.14	15.3	23.2	1018.5	290.7	254.8	-7.69	-5.38	8.3	7.7
<i>Northern cell</i>																
Jan	30.0	-5.0	35.0	3.0	1.3	4.5	0.28	11.0	21.9	1019.6	285.6	254.7	-9.28	-9.23	13.0	7.8
Feb	30.0	-5.0	35.0	2.8	1.1	4.1	0.29	11.0	21.7	1018.6	286.2	254.7	-8.35	-9.34	12.7	7.8
Mar	30.0	-2.5	32.5	2.8	1.1	3.9	0.27	11.7	21.1	1017.8	288.1	255.4	-7.57	-8.86	11.0	7.2
Apr	32.5	2.5	30.0	2.8	1.4	3.9	0.24	12.2	21.0	1016.7	288.3	255.2	-6.53	-8.01	11.1	7.7
May	32.5	7.5	25.0	3.1	1.8	4.1	0.19	14.4	21.1	1015.6	291.3	257.7	-5.00	-6.70	8.3	5.1
Jun	35.0	15.0	20.0	2.6	2.2	2.9	0.07	16.3	21.3	1015.1	292.5	259.6	-4.38	-2.54	8.0	3.4
Jul	37.5	17.5	20.0	2.7	2.1	3.2	0.10	18.2	21.3	1014.8	294.7	260.8	-4.09	-4.14	5.8	2.0
Aug	40.0	17.5	22.5	2.9	2.0	3.5	0.13	17.6	21.1	1014.9	294.8	260.3	-4.43	-4.85	5.7	2.6
Sep	40.0	15.0	25.0	3.1	2.1	3.8	0.14	15.0	20.9	1016.5	291.9	258.1	-5.80	-5.08	8.3	4.4
Oct	37.5	10.0	27.5	3.5	2.1	4.7	0.20	13.3	21.4	1018.4	288.6	255.6	-7.45	-6.85	10.7	6.7
Nov	35.0	5.0	30.0	3.5	1.9	4.7	0.21	11.7	20.7	1020.1	285.5	253.8	-9.63	-6.93	13.3	8.7
Dec	30.0	0.0	30.0	3.1	1.5	4.4	0.24	12.1	21.7	1020.0	287.1	255.6	-9.71	-8.12	11.4	6.9
Ann	32.5	5.0	27.5	3.4	2.0	4.7	0.20	14.1	22.1	1017.0	290.0	257.1	-6.11	-7.41	9.0	5.4

Table 2: Slope values C and squared correlation coefficients R^2 (in braces) for Reduced Major Axis regressions of ΔT_s on ΔT_a ($\Delta T_{si} = C\Delta T_{ai}$), $\Delta T_{si} \equiv T_{si} - \bar{T}_s$, $\Delta T_{ai} \equiv T_{ai} - \bar{T}_a$ where X_i ($X = T_a, T_s$) is the value of X in the i -th gridpoint and \bar{X} is the tropical mean value of X (between 27.5°S and 27.5°N as in (Bayr and Dommenges, 2013)) in a given month or annually averaged. N is the number of gridpoints analyzed.

	Total tropics ($N = 3312$)	Ocean ($N = 2476$)	Land ($N = 836$)
Jan	2.1 (0.49)	1.5 (0.57)	2.5 (0.71)
Feb	2.0 (0.49)	1.5 (0.63)	2.4 (0.64)
Mar	1.9 (0.47)	1.5 (0.69)	2.6 (0.47)
Apr	1.8 (0.48)	1.4 (0.72)	2.8 (0.43)
May	1.8 (0.55)	1.3 (0.69)	2.6 (0.62)
Jun	1.8 (0.60)	1.4 (0.67)	2.4 (0.73)
Jul	1.8 (0.62)	1.5 (0.68)	2.2 (0.75)
Aug	1.8 (0.61)	1.6 (0.67)	2.2 (0.69)
Sep	1.8 (0.56)	1.6 (0.64)	2.3 (0.53)
Oct	1.8 (0.46)	1.6 (0.62)	2.8 (0.30)
Nov	1.9 (0.39)	1.6 (0.59)	2.9 (0.36)
Dec	2.1 (0.44)	1.5 (0.57)	2.7 (0.61)
Annual	1.8 (0.44)	1.5 (0.65)	2.8 (0.46)

References

- An, S.-I., 2011: Atmospheric responses of Gill-type and Lindzen-Nigam models to global warming. *J. Climate*, **24**, 6165–6173, doi:10.1175/2011JCLI3971.1.
- Back, L. E. and C. S. Bretherton, 2009: On the relationship between SST gradients, boundary layer winds, and convergence over the tropical oceans. *J. Climate*, **22**, 4182–4196, doi:10.1175/2009JCLI2392.1.
- Bates, J. R., 1999: A dynamical stabilizer in the climate system: a mechanism suggested by a simple model. *Tellus*, **51A**, 349–372.
- Bates, J. R., 2012: Climate stability and sensitivity in some simple conceptual models. *Climate Dyn.*, **38**, 455–473, doi:10.1007/s00382-010-0966-0.
- Bayr, T. and D. Dommenges, 2013: The tropospheric land-sea warming contrast as the driver of tropical sea level pressure changes. *J. Climate*, **26**, 1387–1402.
- Caballero, R., 2001: Surface wind, subcloud humidity and the stability of the tropical climate. *Tellus*, **53A**, 513–525.
- Dima, I. M. and J. M. Wallace, 2003: On the seasonality of the Hadley Cell. *J. Atmos. Sci.*, **60**, 1522–1527, doi:10.1175/1520-0469(2003)060<1522:OTSOTH>2.0.CO;2.
- Hagemann, S., C. Chen, J. O. Haerter, J. Heinke, D. Gerten, and C. Piani, 2011: Impact of a statistical bias correction on the projected hydrological changes obtained from three GCMs and two hydrology models. *J. Hydrometeor.*, **12**, 556–578, doi:10.1175/2011JHM1336.1.
- Herman, B., M. Barlage, T. N. Chase, and R. A. Pielke Sr., 2008: Update on a proposed mechanism for the regulation of minimum midtropospheric and surface temperatures in the Arctic and Antarctic. *J. Geophys. Res.*, **113**, D24 101, doi:10.1029/2008JD009799.
- Holloway, C. E. and J. D. Neelin, 2010: Temporal relations of column water vapor and tropical precipitation. *J. Atmos. Sci.*, **67**, 1091–1105.
- Huang, P., S.-P. Xie, K. Hu., G. Huang, and R. Huang, 2013: Patterns of the seasonal response of tropical rainfall to global warming. *Nature Geosci.*, **6**, 357–361, doi:10.1038/ngeo1792.
- Johnson, R. H., T. M. Rickenbach, S. A. Rutledge, P. E. Ciesielski, and W. H. Schubert, 1999: Trimodal characteristics of tropical convection. *J. Climate*, **12**, 2397–2418, doi:10.1175/1520-0442(1999)012<2397:TCOTC>2.0.CO;2.
- Kalnay, E., et al., 1996: The NCEP/NCAR 40-year reanalysis project. *Bull. Amer. Meteor. Soc.*, **77**, 437–471.
- Lindzen, R. S. and S. Nigam, 1987: On the role of sea surface temperature gradients in forcing low-level winds and convergence in the tropics. *J. Atmos. Sci.*, **44**, 2418–2436.
- Makarieva, A. M. and V. G. Gorshkov, 2007: Biotic pump of atmospheric moisture as driver of the hydrological cycle on land. *Hydrol. Earth Syst. Sci.*, **11**, 1013–1033.
- Makarieva, A. M. and V. G. Gorshkov, 2010: The biotic pump: Condensation, atmospheric dynamics and climate. *Int. J. Water*, **5**, 365–385.
- Makarieva, A. M. and V. G. Gorshkov, 2011: Radial profiles of velocity and pressure for condensation-induced hurricanes. *Phys. Lett. A*, **375**, 1053–1058.

- Makarieva, A. M., V. G. Gorshkov, and A. V. Nefiodov, 2014a: Condensational power of air circulation in the presence of a horizontal temperature gradient. *Phys. Lett. A*, **378**, 294–298, doi:j.physleta.2013.11.019.
- Makarieva, A. M., V. G. Gorshkov, A. V. Nefiodov, D. Sheil, A. D. Nobre, P. Bunyard, and B.-L. Li, 2013a: The key physical parameters governing frictional dissipation in a precipitating atmosphere. *J. Atmos. Sci.*, **70**, 2916–2929.
- Makarieva, A. M., V. G. Gorshkov, D. Sheil, A. D. Nobre, P. Bunyard, and B.-L. Li, 2014b: Why does air passage over forest yield more rain? Examining the coupling between rainfall, pressure, and atmospheric moisture content. *J. Hydrometeor.*, **15**, 411–426, doi:10.1175/JHM-D-12-0190.1.
- Makarieva, A. M., V. G. Gorshkov, D. Sheil, A. D. Nobre, and B.-L. Li, 2013b: Where do winds come from? A new theory on how water vapor condensation influences atmospheric pressure and dynamics. *Atmos. Chem. Phys.*, **13**, 1039–1056.
- Mapes, B. E., 2001: Water’s two height scales: The moist adiabat and the radiative troposphere. *Quart. J. Roy. Meteor. Soc.*, **127**, 2353–2366, doi:10.1002/qj.49712757708.
- Marengo, J. A., 2006: On the hydrological cycle of the Amazon Basin: A historical review and current state-of-the-art. *Rev. Bras. MeteorHydro.*, **21**, 1–19.
- Mears, C. A. and F. J. Wentz, 2009: Construction of the Remote Sensing Systems V3.2 atmospheric temperature records from the MSU and AMSU microwave sounders. *J. Atmos. Oceanic Technol.*, **26**, 1040–1056, doi:10.1175/2008JTECHA1176.1.
- Montgomery, M. T., M. M. Bell, S. D. Aberson, and M. L. Black, 2006: Hurricane Isabel (2003): New insights into the physics of intense storms. Part I: Mean vortex structure and maximum intensity estimates. *Bull. Amer. Meteor. Soc.*, **87**, 1335–1347, doi:10.1175/BAMS-87-10-1335.
- Neelin, J. D., 1989: On the interpretation of the Gill model. *J. Atmos. Sci.*, **46**, 2466–2468.
- Ramanathan, V. and W. Collins, 1991: Thermodynamic regulation of ocean warming by cirrus clouds deduced from observations of the 1987 El Niño. *Nature*, **351**, 27–32.
- Schneider, T., 2006: The general circulation of the atmosphere. *Annu. Rev. Earth Planet. Sci.*, **34**, 655–688.
- Schubert, W. H., P. E. Ciesielski, C. Lu, and R. H. Johnson, 1995: Dynamical adjustment of the trade wind inversion layer. *J. Atmos. Sci.*, **52**, 2941–2952, doi:10.1175/1520-0469(1995)052<2941:DAOTTW>2.0.CO;2.
- Sharkov, E. A., Y. N. Shramkov, and I. V. Pokrovskaya, 2012: Increased water-vapor content in the atmosphere of tropical latitudes as a necessary condition for the genesis of tropical cyclones. *Izvestiya Atmos. Ocean. Phys.*, **48**, 900–908.
- Sobel, A. H. and J. D. Neelin, 2006: The boundary layer contribution to intertropical convergence zones in the quasi-equilibrium tropical circulation model framework. *Theor. Comput. Fluid Dyn.*, **20**, 323–350, doi:10.1007/s00162-006-0033-y.
- Stevens, B., J. Duan, J. C. McWilliams, M. Münnich, and J. D. Neelin, 2002: Entrainment, Rayleigh friction, and boundary layer winds over the tropical Pacific. *J. Climate*, **15**, 30–44.

- Tokinaga, H., S.-P. Xie, A. Timmermann, S. McGregor, T. Ogata, H. Kubota, and Y. M. Okumura, 2012: Regional patterns of tropical Indo-Pacific climate change: Evidence of the Walker circulation weakening. *J. Climate*, **25**, 1689–1710, doi:10.1175/JCLI-D-11-00263.1.
- Wallace, J. M., 1992: Effect of deep convection on the regulation of tropical sea surface temperature. *Nature*, **357**, 230–231.

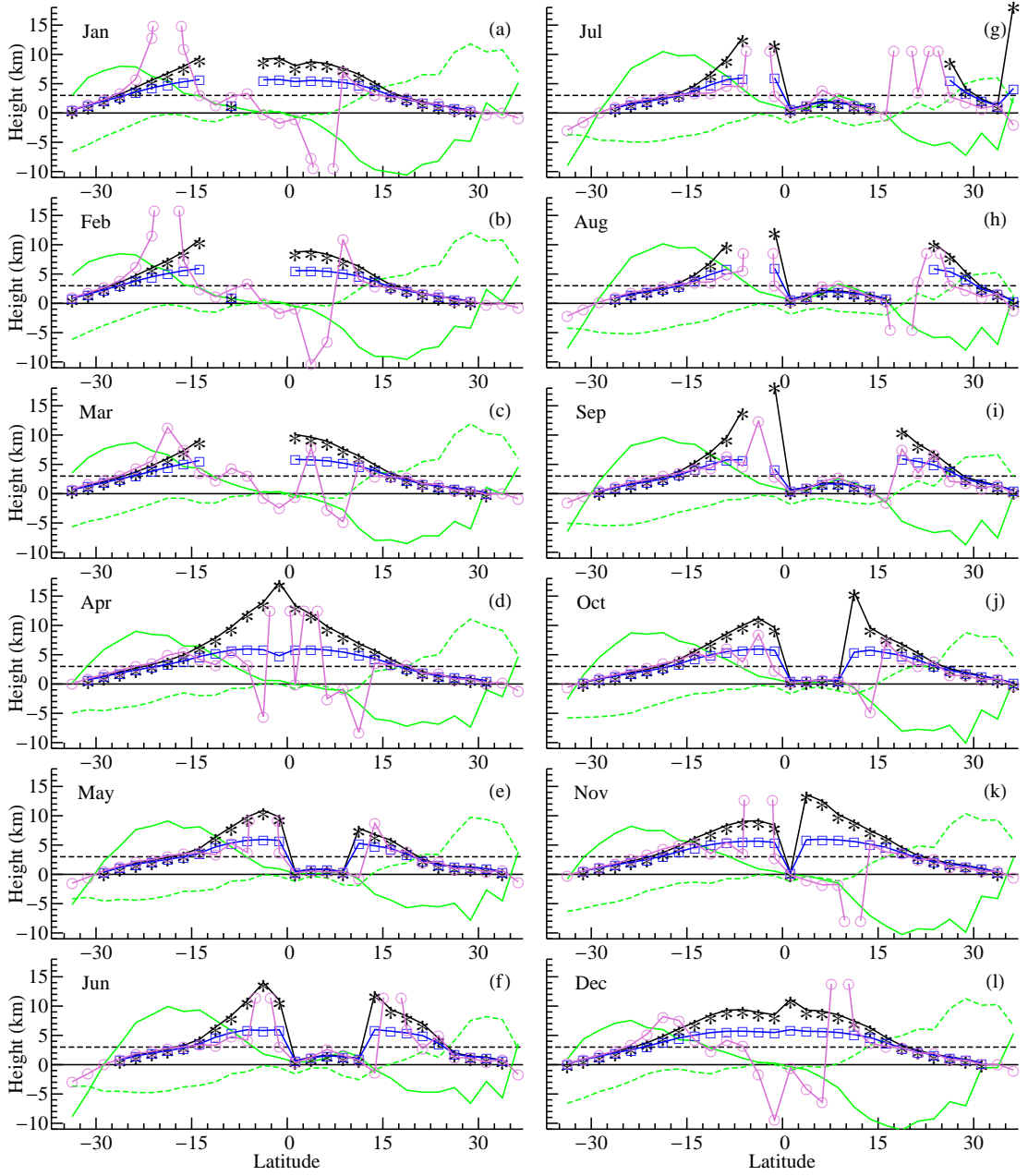


Figure 1: The observed isobaric height $z_e \equiv Z_e h_s$ (black curve with asterisks) (the height where the meridional pressure gradient $\partial p(z_e)/\partial y = 0$), the observed ratio of the meridional gradients of SLP and surface air temperature $-(da/db)h_s = -(\partial p_s/\partial y)/(\partial T_s/\partial y)(T_s/p_s)h_s$ (purple curve with open circles) and its theoretical estimate (12) with isothermal height $z_i \equiv Z_i h_s = 12$ km (blue curve with open squares). Missing points indicate latitudes where the meridional pressure gradient does not change its sign anywhere between the 1000 hPa and 70 hPa pressure levels. Green curves show (minus one times) the meridional gradients of SLP (solid, in $0.05 \text{ hPa } (^\circ\text{lat})^{-1}$) and surface air temperature (dashed, in $0.1 \text{ K } (^\circ\text{lat})^{-1}$). The negative values are used to ease readability. Note that the sharp fluctuations in the purple curve correspond to latitudes where the surface temperature gradient is near zero ($db = 0$).

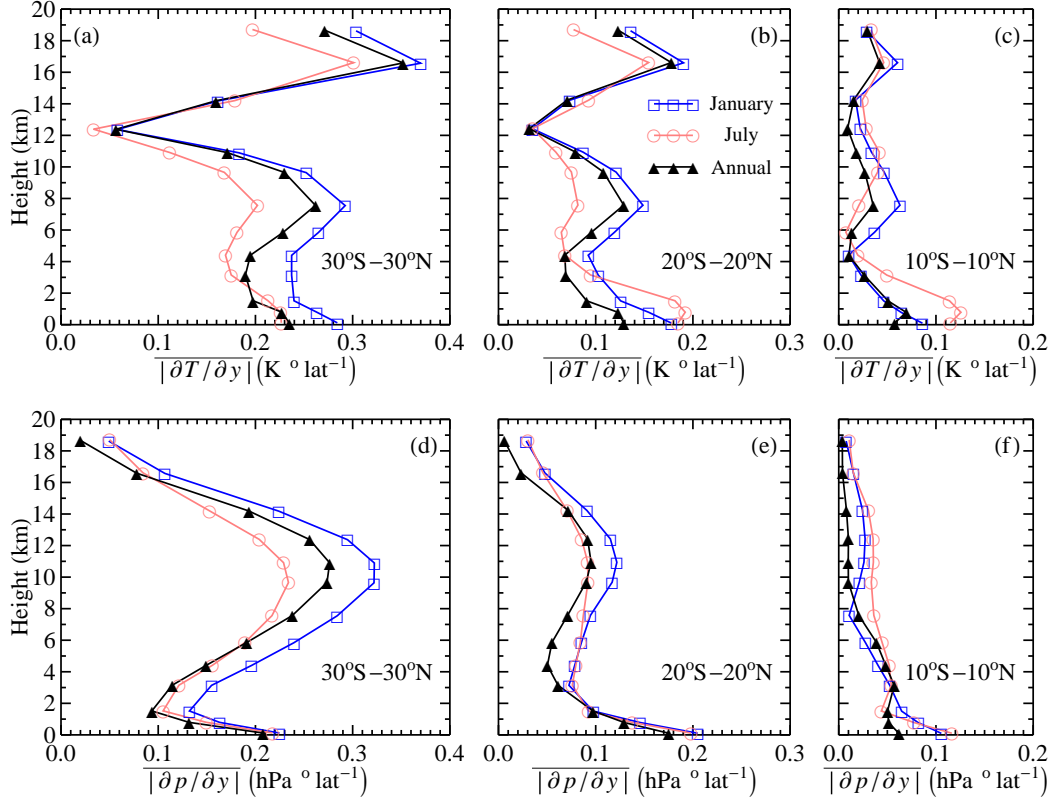


Figure 2: Vertical profiles of the meridional temperature (a-c) and pressure (d-f) gradients taken by absolute magnitude and averaged from 30°S to 30°N (a,d), 20°S to 20°N (b,e) and 10°S to 10°N (c,f) in January (blue squares), July (pink circles) and annually (black triangles). The pantropical constant isothermal height $z_i \approx 12$ km corresponds to a minimum of $|\partial T/\partial y|$ that is practically independent of the averaging area. In contrast, height of the minimum pressure gradient in the lower atmosphere moves upwards from less than 2 km (d) to 8–10 km (f) as the averaging area decreases. This reflects the growth of isobaric height towards the equator (cf. Fig. 1a,g).

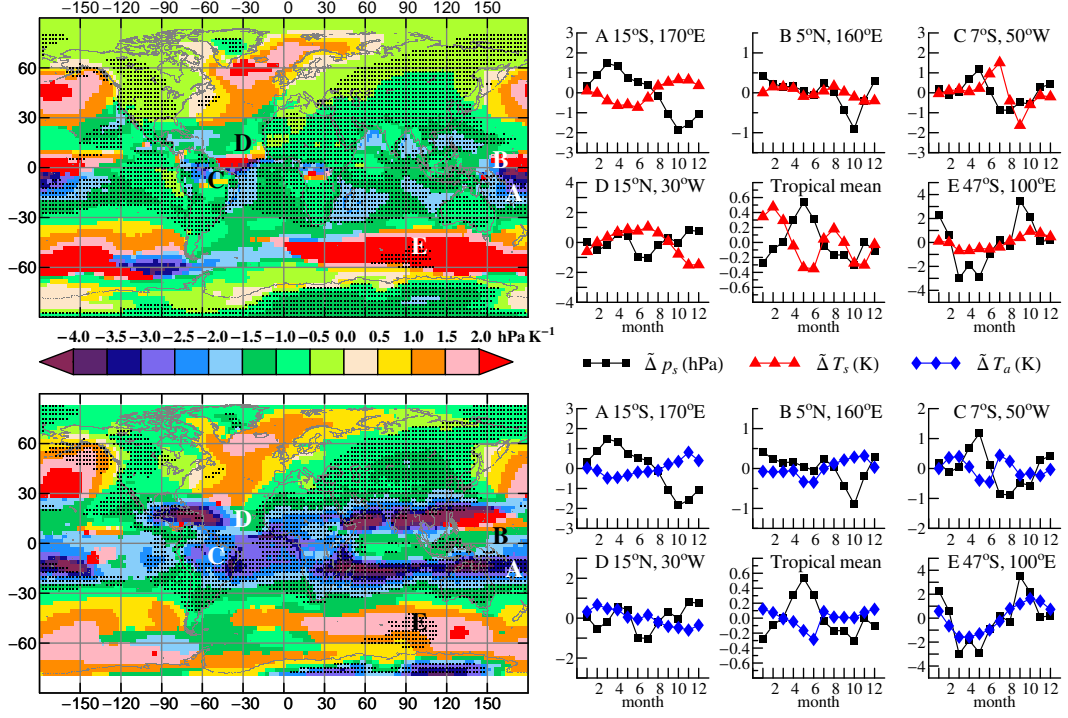


Figure 3: Mean ratio between local monthly changes of SLP p_s and surface temperature T_s (larger top left panel) and SLP and tropospheric temperature T_a (larger lower left panel). The ratio is estimated as the slope coefficient of a Reduced Major Axis regression of $\tilde{\Delta} p_s \equiv p_s(m_2) - p_s(m_1)$ on, respectively, $\tilde{\Delta} T_s \equiv T_s(m_2) - T_s(m_1)$ and $\tilde{\Delta} T_a \equiv T_a(m_2) - T_a(m_1)$, where $\tilde{\Delta} p_s$, $\tilde{\Delta} T_s$ and $\tilde{\Delta} T_a$ are the monthly changes of the respective variables between two consecutive months m_1 and m_2 . Black dots indicate where the probability level of the regression is less than 0.01. The small panels exemplify seasonal changes of $\tilde{\Delta} p_s$, $\tilde{\Delta} T_s$ and $\tilde{\Delta} T_a$ in individual grid points (A, B, C, D and E) shown in the big panels, as well as the tropical mean (the area between 27.5°S and 27.5°N). Note the different vertical scales in the small panels. Tropical mean (\pm standard deviation) of the obtained local slope coefficients are -1.1 ± 1.0 hPa K⁻¹ (land -0.98 ± 0.62 hPa K⁻¹, ocean -1.09 ± 1.11 hPa K⁻¹) and -2.0 ± 1.3 hPa K⁻¹ (land -2.2 ± 0.8 hPa K⁻¹, ocean -1.9 ± 1.4 hPa K⁻¹) for the larger upper and lower panels, respectively.

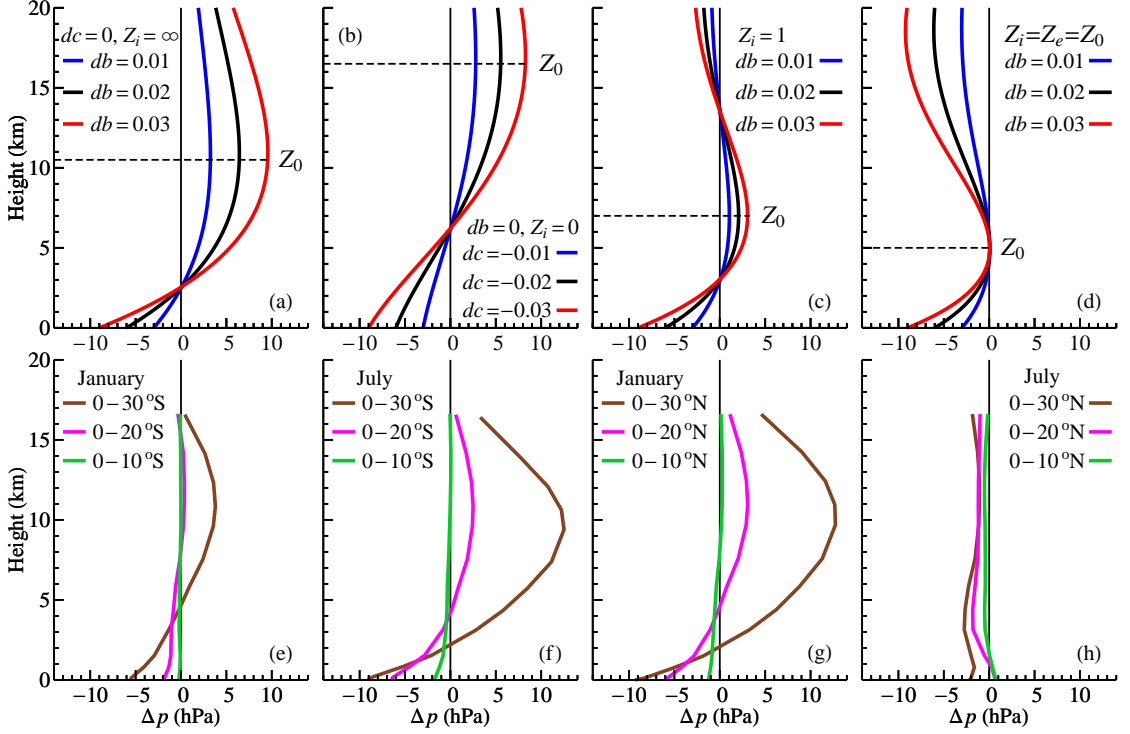


Figure 4: Vertical profiles of pressure differences $\Delta p(z)$ between air columns differing in their lapse rate, surface pressure and temperature. Panels (a)-(d): theoretical profiles (10) with $dp = \Delta p$, $da = \Delta p_s/p_s$, $db = \Delta T_s/T_s$, $zdc = \Delta \Gamma/\Gamma_g$ (cf. 11), $p_s = 1000$ hPa, $T_s = 300$ K. In panels (a)-(d) $da = -0.003$, -0.006 , -0.009 for the blue, black and red curves, respectively. In each panel $da/db = \text{constant}$ for all the three curves. Dashed line Z_0 (19) shows the height where the positive pressure difference in the upper atmosphere is maximum, $\Delta p(Z_0) = \Delta p_0$ (20). Note two isobaric heights in panel (c). In panel (d) note that condition $Z_i = Z_0$ (the atmosphere is horizontally isothermal where the positive pressure difference aloft is maximum) yields $Z_i = Z_0 = Z_e = -2da/db = (-2da/dc)^{1/2}$, see (12), (19) and (14), and $\Delta p_0 = 0$, i.e. the pressure surplus aloft disappears. Panels (e)-(h): real vertical profiles of zonal averages between the air columns at the equator and the 10th, 20th and 30th latitudes in the Southern (e,f) and Northern (g,h) hemispheres in January (e,g) and July (f,h). E.g., the brown line in (e) shows the difference between the air column at the equator and at 30°S in January. Note that while the theoretical curves (a-d) in each panel are chosen such that they have one and the same isobaric height Z_e (i.e., they cross the line $\Delta p = 0$ at the same point), this varies for the real profiles (e-h).

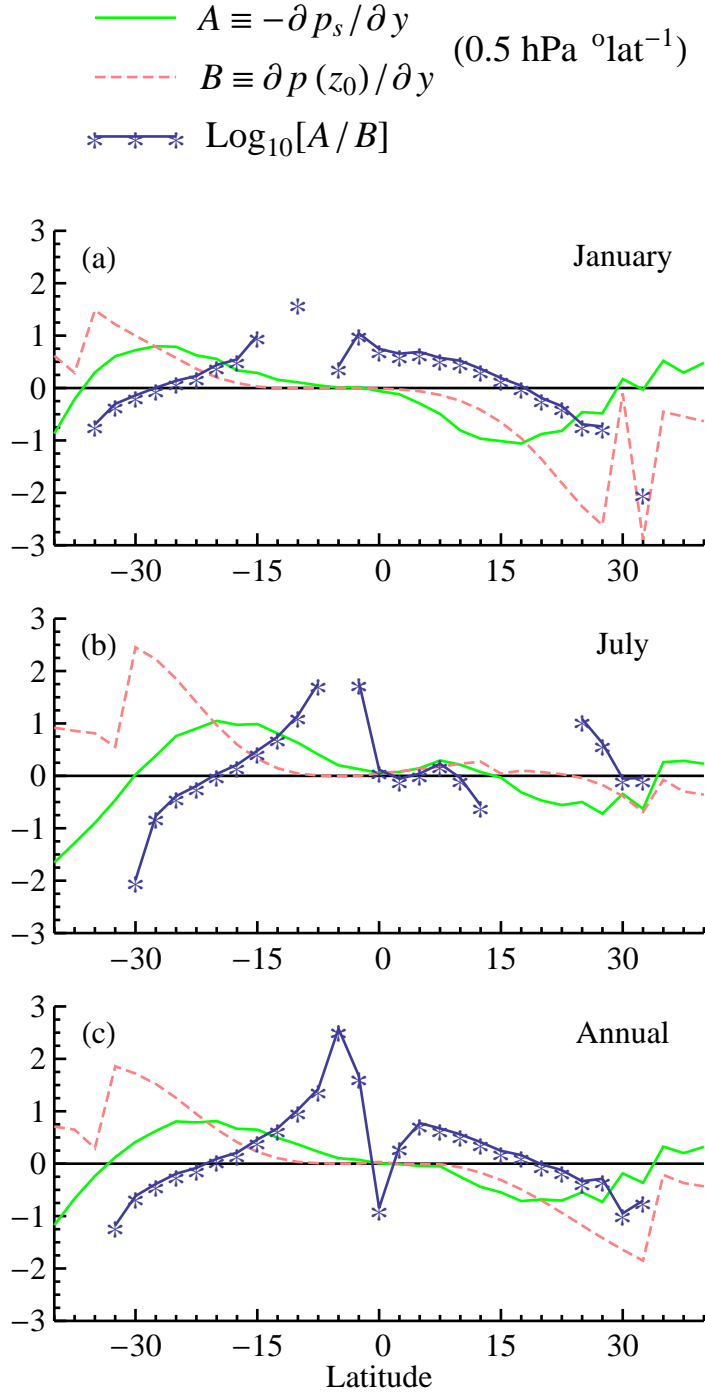


Figure 5: Logarithm of the ratio of the meridional gradient of SLP taken with the minus sign $A \equiv -\partial p_s / \partial y$ to the meridional pressure gradient in the upper atmosphere $B \equiv \partial p(z_0) / \partial y$. B is calculated as the pressure difference Δp_0 at $z = z_0$ (20) between two neighboring latitudes divided by 2.5° : z_0 is the height where $|\partial p(z) / \partial y - \partial p_s / \partial y|$ is maximum at a given y . Missing values indicate latitudes where A and B are of different sign (and there is thus no isobaric height in the troposphere, cf. Fig. 1a,g).

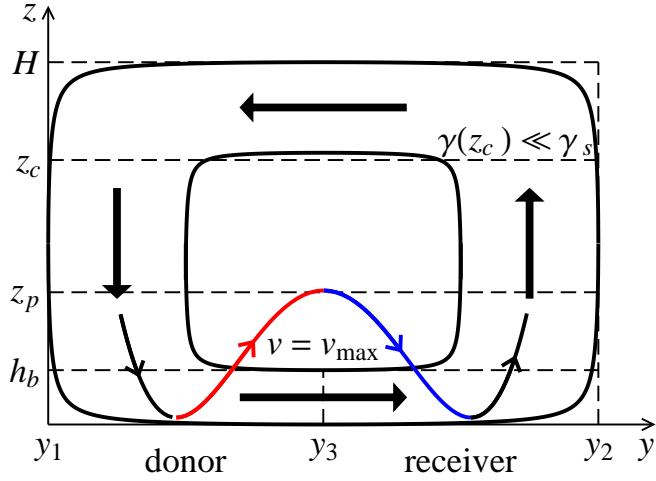


Figure 6: Donor and receiver areas. Thick arrows indicate large-scale air flows. Condensation occurs in the receiver area at $h_b \leq z \leq z_c$. Thin arrows indicate turbulent eddies accompanying the large-scale flow with air parcels rising in the donor area with a low (moist adiabatic) lapse rate (red curve) and descending in the receiver area with a higher (dry adiabatic) lapse rate (blue curve). See text for other details.

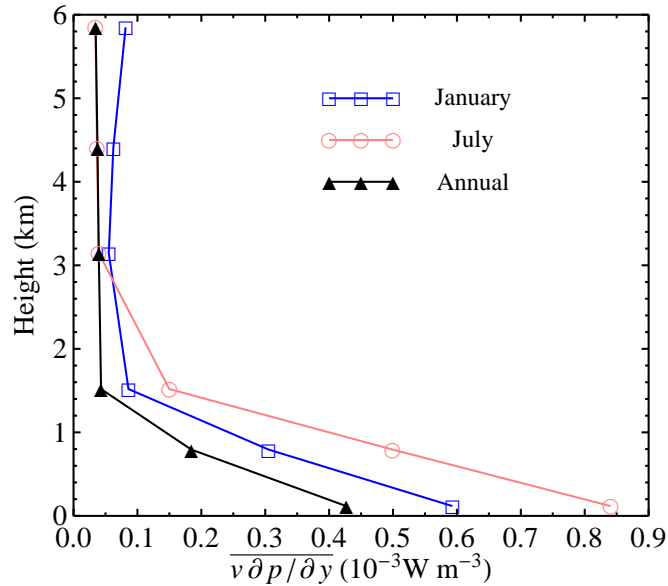


Figure 7: Tropical mean vertical profiles of the product of meridional velocity and meridional pressure gradient in the lower atmosphere in January, July, and annually averaged. Profiles constructed by calculating $v \partial p / \partial y$ in each gridpoint at different pressure levels as described and then averaging from 30°S to 30°N . Monthly data from NCAR-NCEP reanalysis averaged for 1978-2013 (see Section 4 for more details).

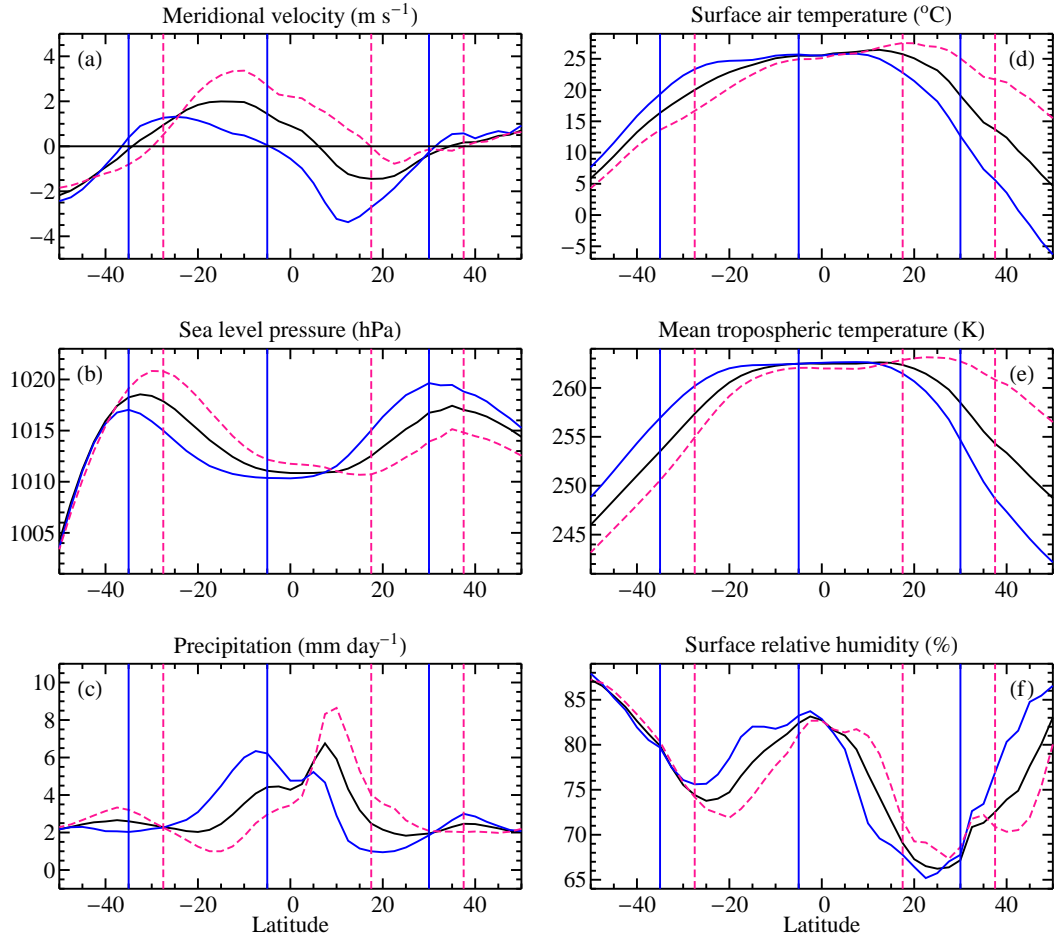


Figure 8: Zonally averaged atmospheric parameters of Hadley cells. Solid black curve: annually averaged data, solid blue curve: January, dashed pink curve: July. Vertical lines show the borders of the Southern and Northern cells in January (solid blue) and July (dashed pink). These borders are defined as latitudes where meridional velocity is zero (a). They simultaneously coincide with the two poleward maxima (the outer borders) and the central minimum (the inner border) of SLP (b). Monthly data from NCAR-NCEP reanalysis averaged for 1978-2013 (see Section 4 for more details).

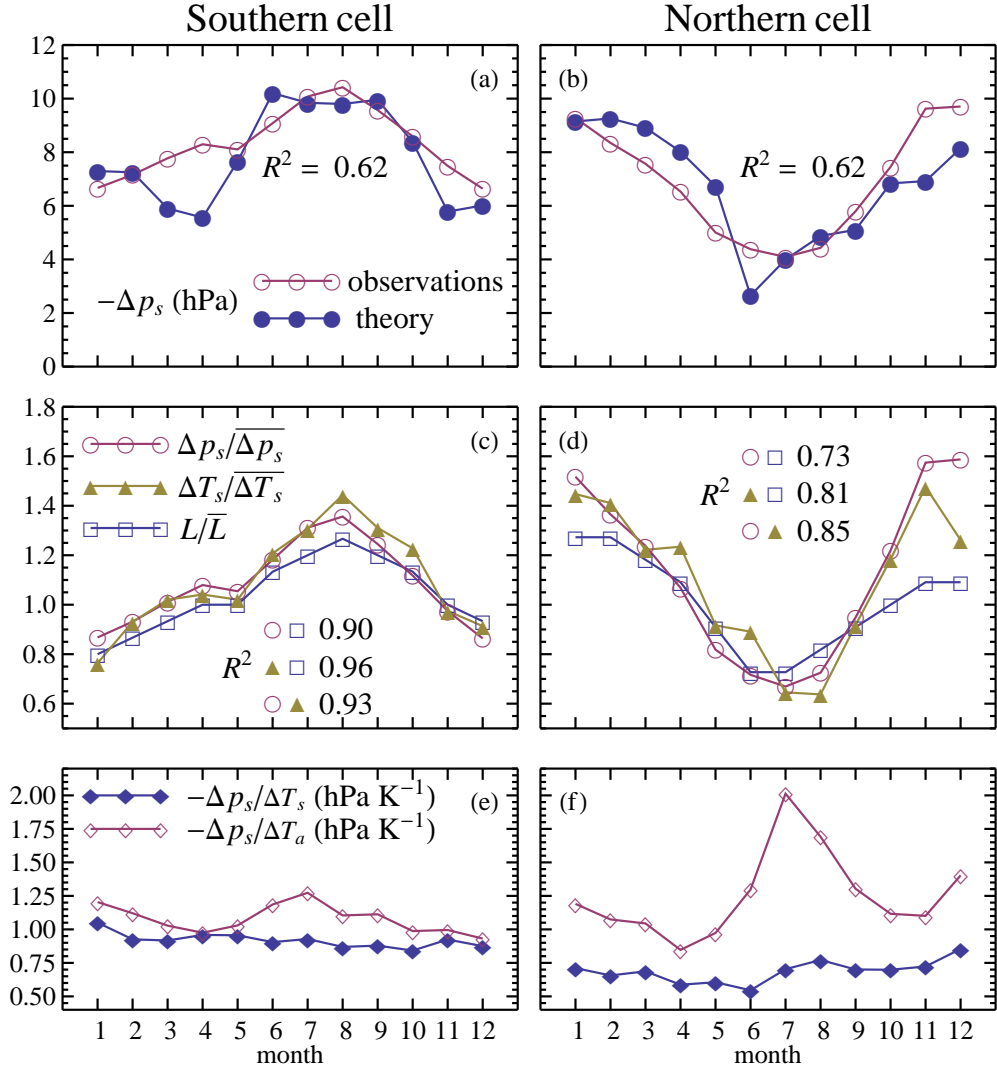


Figure 9: Seasonal dynamics of pressure and temperature differences across the Southern (a,c,e) and Northern (b,d,f) Hadley cells. a,b: observed and theoretically estimated from Eq. (30) SLP differences $-\Delta p_s \equiv p_s(y_1) - p_s(y_2) \equiv p_{s1} - p_{s2}$ and the squared correlation coefficient for the ordinary least square regression between them. c,d: Relative changes of SLP and temperature differences Δp_s and ΔT_s and cell length L (all divided by their annual mean values denoted by overbar). Squared correlation coefficients for the pairwise ordinary least square regressions between the variables are also shown. e,f: Ratios of SLP difference to surface temperature T_s and mean tropospheric temperature T_a differences. See Table 1 for all numerical values.

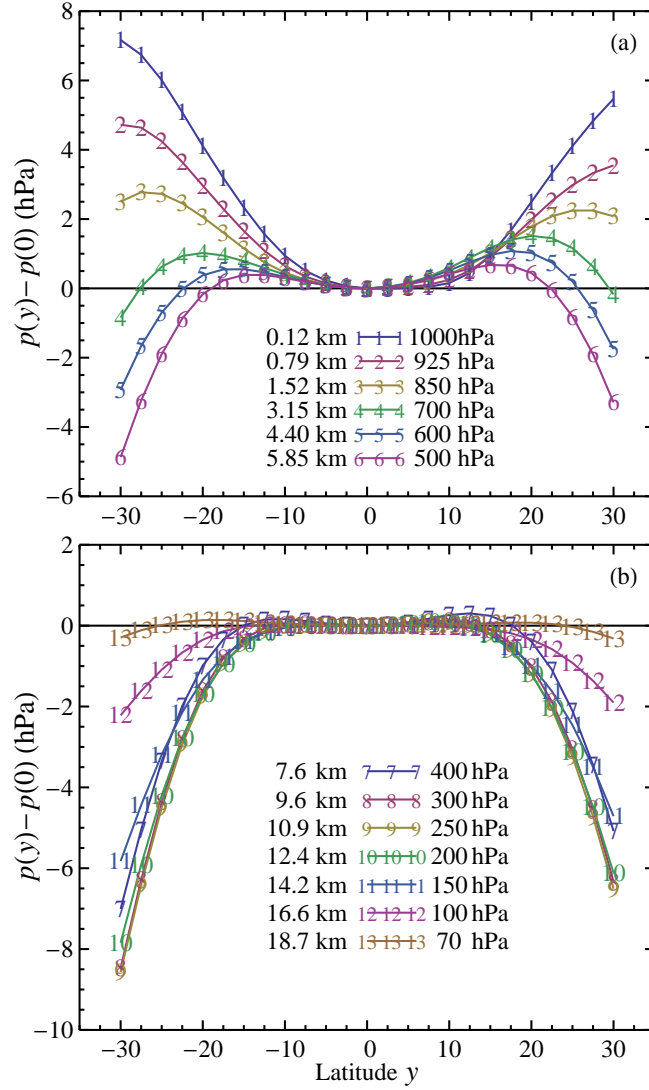


Figure 10: Annual mean difference $p(y) - p(0)$ between pressure at latitude y and the equator at different heights. E.g. curve 1 in (a) shows meridional pressure variation at height $z = 0.12$ km, which is equal to the tropical mean geopotential height of pressure level 1000 hPa. Note that the pressure difference between the 30th latitudes and the equator approaches zero for $z = 3.15$ km (pressure level 700 hPa). Monthly data from NCAR-NCEP reanalysis averaged for 1978-2013 (see Section 4 for more details).

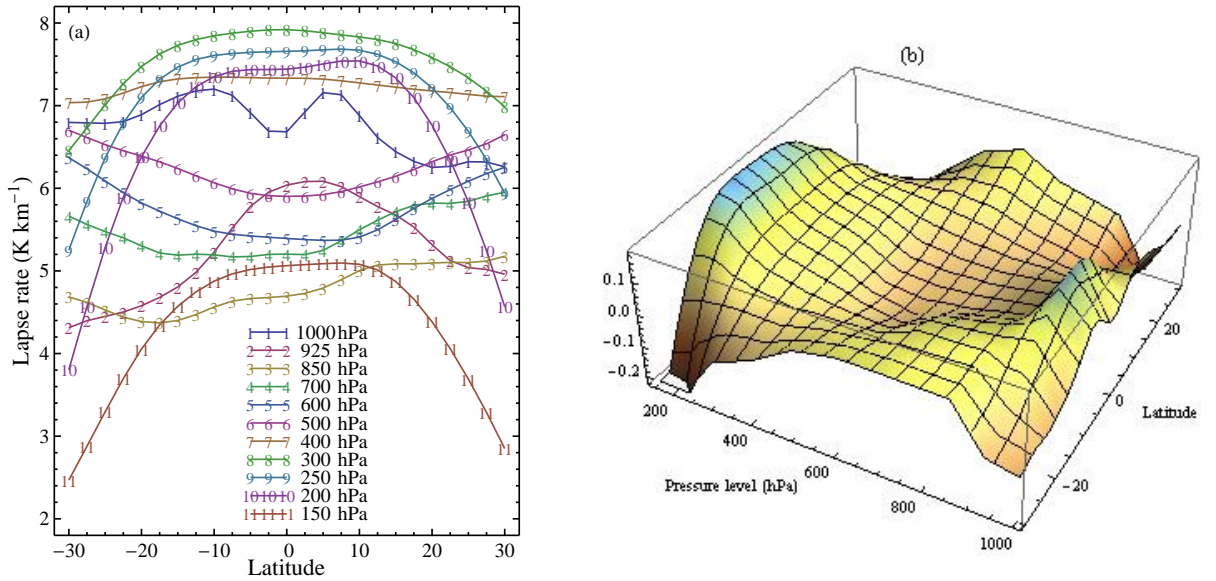


Figure 11: Annual mean latitudinal profiles of the air temperature lapse rate on different pressure levels. For example, curve 1 in (a) shows the mean lapse rate between 1000 hPa and 925 hPa; curve 2 — between 925 hPa and 850 hPa; curve 11 — between 150 and 100 hPa. The tropical mean lapse rate (the temperature difference between 1000 hPa and 100 hPa levels divided by the difference in the geopotential heights and averaged from 30°S to 30°N) is 6.0 K km^{-1} . Panel (b) shows the relative variation — at each pressure level the lapse rate at a given latitude is divided by the mean lapse rate at this level (averaged between 30°S and 30°N). The equator has a higher lapse rate than the 30th latitudes in the lower and upper — but not the middle — troposphere.